

POLITECNICO DI TORINO

Master's Degree in Energy and Nuclear Engineering



**Politecnico
di Torino**

Master's Degree Thesis

***PERFORMANCE SIMULATIONS OF
PROTON EXCHANGE MEMBRANE
FUEL CELLS IN DIFFERENT
TEMPERATURE AND MOISTURE
CONDITIONS***

Supervisors

Prof. Alessandro Hugo Antonio MONTEVERDE

Prof. Massimo SANTARELLI

Candidate

Enrico COLORE

December 2021

Acknowledgements

To all those who have been close to me during these five years.

To the efforts I made over the years.

To the desire residing somewhere inside me to change this world in some way,
may it continue to guide me after this experience.

I hope someday I will reread this work with the consciousness of having been part of it in
some way.

Abstract

Proton exchange membrane fuel cells are becoming more relevant especially in the automotive sector given the new transition underway towards electric. In the introduction there is a brief explanation of the state of art of fuel cell sector, the principal automotive solutions available today, how polarization curve is obtained and the importance of catalyst deposition to improve cell performance. This is followed by an explanation of the COMSOL model used to execute the cell performance simulations with all equations that govern it. After this first explanation, I provide some ionomer ink preparations in the laboratory of Politecnico, analysing how temperature can influence the mixing procedure. Furthermore, using some reference experimental parameters, I changed some of them related to the ionomer section in order to parametrize it and modified it to run the simulations. This process is necessary to evaluate five different membranes and to perform some simulations for them under different temperature and moisture conditions. The reference membrane was Nafion 211 and I compared this one with other Solvay membranes. The most performing one is the Solvay Aquivion E87 which shows high results compared to the other four typologies. The simulation analysis was conducted by mainly comparing the polarization curves with the main electrical parameters. Considering the full power of the model, I also conducted an analysis of the simulations related to current distribution and oxygen transport. With these simulations I evaluated the results motivating them and comparing them with the results that were available in the literature.

Index:

List of figures	Pag. 4
List of tables	Pag. 6
1. Introduction	Pag. 7
1.1. <i>State of art of current fuel cell technologies</i>	Pag. 7
1.2. <i>Global context</i>	Pag. 10
1.3. <i>State of art in automotive sector</i>	Pag. 13
1.4. <i>Polarization Curve</i>	Pag. 14
1.5. <i>Future Development</i>	Pag. 16
1.6. <i>Catalyst deposition</i>	Pag. 17
2. Model explanation	Pag. 20
2.1. <i>How does it work?</i>	Pag. 20
2.2. <i>Analytical explanation</i>	Pag. 21
2.2.1. <i>Electrochemistry equations</i>	Pag. 21
2.2.2. <i>Heat/mass transport equations</i>	Pag. 22
2.2.3. <i>Phase transitions equations</i>	Pag. 23
2.2.4. <i>Parametrizations</i>	Pag. 25
2.2.5. <i>Principal ionomer parameters</i>	Pag. 26
3. Reference model evaluation	Pag. 28
4. Experimental procedure	Pag. 35
4.1. <i>Experimental preparation procedures</i>	Pag. 35
4.2. <i>Catalyst performance evaluation at different temperature conditions</i>	Pag. 39
5. COMSOL cell comparison	Pag. 41
5.1. <i>Typology of membrane evaluated</i>	Pag. 41
5.2. <i>Constant temperature simulations</i>	Pag. 46

5.2.1. 80°C and 25% RH	Pag. 46
5.2.2. 80°C and 50% RH	Pag. 47
5.2.3. 80°C and 75% RH	Pag. 49
5.2.4. 80°C and 100% RH	Pag. 50
5.3. <i>Constant relative humidity simulations</i>	Pag. 53
5.3.1. 90% RH and 30 °C	Pag. 53
5.3.2. 90% RH and 50 °C	Pag. 54
5.3.3. 90% RH and 70 °C	Pag. 56
5.3.4. 90% RH and 80 °C	Pag. 57
5.4. Simulation validation through literature comparison	Pag. 59
5.5. Simulation analysis	Pag. 61
5.5.1 Current distribution	Pag. 62
5.5.2 Oxygen transport	Pag. 65
5.5.3 Water transport	Pag. 71
5.6. Proposals for enhancing cell parameters	Pag. 76
6. Conclusions	Pag. 78
7. References	Pag. 80

List of figures

Figure 1 - PEMFC internal scheme.

Figure 2 - CO₂ emissions by source.

Figure 3 - Global CO₂ emissions by years.

Figure 4 - Typical FC polarization curve.

Figure 5 - Catalyst deposition.

Figure 6 - Ball milling and hydrodynamic cavitation.

Figure 7 - Catalyst deposition comparison.

Figure 8 - MATLAB model representation.

Figure 9 - Test condition T1.

Figure 10 - Model validation for test T1

Figure 11 - Model validation for test T3

Figure 12- Electric potential.

Figure 13 - Electrolyte potential.

Figure 14 - Temperature distribution.

Figure 15 - Water molar fraction.

Figure 16 - Hydrogen molar fraction.

Figure 17 - Oxygen molar fraction.

Figure 18 - Total heat flux.

Figure 19 - Hydrogen gas flux.

Figure 20 - Oxygen gas flux.

Figure 21 - Ink sonification

Figure 22 - Ink deposition

Figure 23 - Typically cycling polarization curve

Figure 24 - Cycling polarization curve in Lab

Figure 25 - Backward test

Figure 26 - Forward test

Figure 27 - The system used to perform thermostatic measurement

Figure 28 - LSC and SSC

Figure 29 – Ionomers' density variation in function of lambda.

Figure 30 – Ionomers' diffusivity parameters in function of Lambda

Figure 31.A - Polarization curve at 80°C and 25% RH

Figure 31.B - Power density curve at 80°C and 25% RH

Figure 32.A - Polarization curve at 80°C and 50% RH

Figure 32.B - Power density curve at 80°C and 50% RH

Figure 33.A - Polarization curve at 80°C and 75% RH

Figure 33.B - Power density curve at 80°C and 75% RH

Figure 34.A - Polarization curve at 80°C and 100% RH

Figure 34.B - Power density curve at 80°C and 100% RH

Figure 35 - Simulation comparison at 353 K and 100% RH

Figure 36.A - Polarization curve at 90% and 30°C.

Figure 36.B - Aquivion E87, 90% RH and 30°C.

Figure 37.A - Nafion 211, 90% RH and 50°C.
Figure 37.B - Aquivion E87, 90% RH and 50°C.
Figure 38.A - Nafion 211, 90% RH and 70°C.
Figure 38.B - Aquivion E87, 90% RH and 70°C.
Figure 39.A - Nafion 211, 90% RH and 90°C.
Figure 39.B - Aquivion E87, 90% RH and 90°C.
Figure 40 - Simulations validation, polarization curve.
Figure 41 - Simulations validation, power curve.
Figure 42 - Electrode current density, E-87.
Figure 43 - Electrolyte current density, E-87.
Figure 44 - Electrode current density zooms of the cathode catalyst layer, E-87.
Figure 45 - Electrode current density zooms of the cathode catalyst layer, E-87.
Figure 46 - Electrode current density zooms of the cathode catalyst layer, Nafion 211.
Figure 47 - Electrode current density zooms of the cathode catalyst layer, Nafion 211.
Figure 48 - 3D current density distribution example.
Figure 49 - Typical fuel cell model.
Figure 50 - Central part of the cell and Pt/C and ionomer agglomerate.
Figure 51 - Oxygen transport resistance in function of Pt loading.
Figure 52 - Oxygen gas flux E-87.
Figure 53 - Catalyst layer Oxygen flux, E-87.
Figure 54 - Oxygen gas flux, Nafion 211.
Figure 55 - Catalyst layer oxygen flux, Nafion 211.
Figure 56 - Water transport.
Figure 57 - Water gas flux E-87.
Figure 58 - Water gas flux, Nafion 211.
Figure 59 - Water ionomer flux related to catalytic and membrane layers, E-87.
Figure 60 - Water ionomer flux related to catalytic and membrane layers, Nafion 211.
Figure 61 - Liquid water flux, E-87.
Figure 62 - Liquid water flux, Nafion 211.
Figure 63 - Ionomer water content E-87.
Figure 64 - Ionomer water transport validation.

List of tables

Table 1 - Toyota FCs comparison.

Table 2 - New PEMFCs target.

Table 3 - Heat sources generation summarize.

Table 4 - Starting data for model evaluation.

Table 5 - Common test parameters.

Table 6 - Paper and model data comparison.

Table 7 - Membrane characteristics comparison.

Table 8 - Performance comparison of different membranes.

1 INTRODUCTION

This introduction chapter offers a brief overview of the different types of fuel cells that are used, the global context which can favourite their growth, their automotive applications, the polarization curve and its importance in this context, and finally the direction of improvement looking at the different methods of ink deposition.

1.1 State of art of current fuel cell technologies

Our days requires a huge effort to reduce pollutant emissions and one of the best ways to overcome this issue is the electrification of energetic systems. This is a complex theme because electricity requires storage to ensure constant grid supplying but storage systems can be expensive and their demand is drastically growing.

Storage systems are complex world with different technologies but the main one is batteries. Even though this, Fuel Cells (FC) can be considered as parallel solution because energy can be stored also in chemical form within the hydrogen. Fuel Cells are promising solution but they require some improvement.

The actual state of art provides different technologies of FCs with several solutions for various operation condition. They can differ depending on the type of ions transported and the different temperature conditions under which they work:

- *MCFC - Molten Carbonate Fuel Cell* is a type of cell that works at high-temperature (650 °C) using an electrolyte composed of a molten carbonate salt mixture suspended in a porous, chemically inert ceramic lithium aluminium oxide matrix. Some FCs require precious catalyst and one of most important advantage for MCFCs is that they are able to work without it and it's useful to reduce cost and reduce dependency of rare metals. Another big advantage is the possibility to directly use methane or other light hydrocarbons because high temperature provides a process called internal reforming. The most important disadvantage is the corrosive electrolyte that reduce life of cell decreasing performance in a not economic amount of time.

Today the principal application is related to coal and natural gas power plants or some industrial or military applications. It's possible coupling this type of cell with a turbine reaching high level of efficiency (65%) and collecting waste heat we can be improved reaching 85% overall efficiency.[1]

- *AFC - Alkaline Fuel Cell* uses a solution of potassium hydroxide in water as the electrolyte and can use a variety of non-precious metals as a catalyst at the anode and cathode. AFCs are very similar to PEMFCs, but they use alkaline solution instead of acid membrane with not so high working temperature, around 70°C and 120°C.

U.S. uses this kind of FC in space program because they can reach performance above 60% of efficiency. The main problem is the susceptible to poisoning by carbon dioxide (CO₂) even if small amount.[1][2]

- *SOFc - Solid Oxide Fuel Cell* use as electrolyte a hard and non-porous ceramic compound. This kind of FC shows an efficiency around 60% reaching 85% using cogeneration. SOFCs operate at very high temperatures also around 1,000°C and high temperature are required due to removes precious-metal catalyst and to allow internal reforming; this is crucial to reducing system and fuel costs.

SOFCs, among all types of FCs, are also the most sulfur-resistant type and they can maintain their performance in presence of carbon monoxide.

High temperature working condition has some disadvantages too: it results in a slow start up conditions: it can be acceptable for utility applications but not for transportation. High temperature requires specific materials able to withstand thermal stress. [1]

- *PAFC - Phosphoric Acid Fuel Cell* makes use of a liquid phosphoric acid as an electrolyte and porous carbon electrodes containing a platinum catalyst. The main utilization of PAFCs is stationary power generation, but some items are used to power large vehicles as city buses.

PAFCs are more tolerant of carbon monoxide impurities in fossil fuels that have been reformed into hydrogen than PEM cells and the efficiency can overcome 85% when it's coupled to heat recovery (co-generation). Comparing to other FC, PAFCs have lower power density so, as a result, due to reach the same amount of power production it's required larger and heavier cells. It's also an expensive technology because it needs more platinum than PEMFC. [1]

- *DMFC - Direct Methanol Fuel Cell* are powered by pure methanol, usually mixed with water and fed directly to the fuel cell anode. It allows to reduce fuel storage problems thanks to higher energy density of methanol compared to hydrogen. The most common application today is providing power for portable fuel cell applications such as cell phones or laptop computers.[1]

- *PEMFC - Proton Exchange Membrane Fuel Cell* is the type of fuel cell I will analyse in this thesis. PEMFCs use a solid polymer as an electrolyte and porous carbon electrodes containing a platinum or platinum alloy catalyst. It's a typology of cell which needs only hydrogen, oxygen (from the air) and water to operate.

PEMFCs deliver high power density allowing to reduce weight and volume and can operate at relatively low temperatures, around 80°C, allowing quick start up time useful to transport utilization such as cars, buses, but also heavy-duty trucks where some interesting applications already exist today. Low temperature means better durability due to not stressful conditions for materials. However, it requires that a noble-metal catalyst, typically platinum, increasing system cost. [1]

The fuel cells analysed into this work are the PEMFCs therefore is crucial looking at the way they work. They contain membrane electrode assemblies (MEAs), where the electrochemical reactions take place. The MEA is composed by a proton exchange membrane (PEM), catalyst layers (CL), gas diffusion layers (GDL), microporous layers (MPL) and transport porous layers (TPL). These components are produced individually and then pressed together at high temperatures and pressures. The electrodes are made of catalyst inks deposited: this process is crucial to achieving proper optimisation of the catalytic processes.

Catalyst ink is usually deposited by a few specific methods: by either the decal, blade process, screen-printing, painting, spraying (air and ultrasonic), electro-spraying, or electrophoretic method.[3] These processes give different results in polarization curve, as it explains in the following section of this work.

In the figure below (figure 1) is presented the operation scheme of PEMFC.

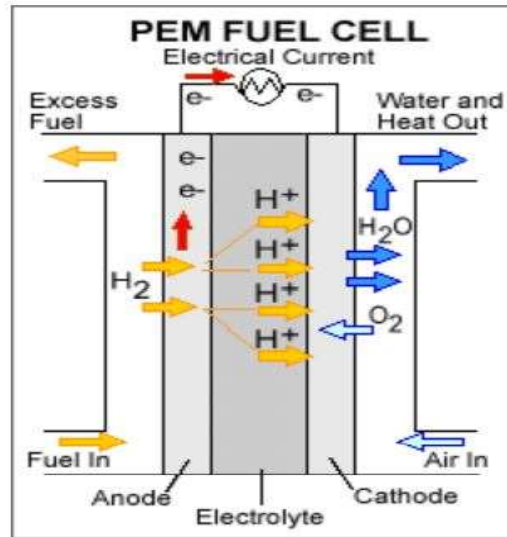
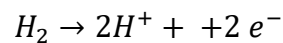
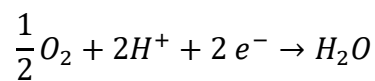


Figure 1 - PEMFC internal scheme [4]

Starting from the left, where the anode of the cell is located, there is the input of the first gas: hydrogen. At the anode, hydrogen is split by the action of the catalyst. This process releases H^+ ions and electricity. The electricity is collected by the external circuit while the hydrogen ion crosses the membrane to recombine at the cathode, where it will form a water molecule.



On the cathode side, there is oxygen input, which is reduced by the activation of the catalyst and the negative charges present.



Once oxygen has been reduced, it can combine with hydrogen ions to form a water molecule. This cycle of reactions is an exothermic cycle, in other words it releases heat.

1.2 Global context

Each new technology that faces global market requires specific boundary conditions that can leave it the space and guarantee the necessary amount of financing to grow, establish itself and subsequently appear autonomously on the global market. Nowadays the best possible scenario to favourite the fuel cell growth is ready. Looking at the last few years, lot of environmental movements were born as an example, Friday for Future in 2018. All these attentions on climate, the scientists voice related to global warming, the sensibilization of people on this problem pushes global government to make some moves.

From the point of view of global meetings there are different meeting held over the years, but the most important one is called Conference of the Parties (COP) that is the supreme decision-making body of the Convention. All States take decisions necessary to promote the effective implementation of the Convention, including institutional and administrative arrangements.[5] Some of these conferences are more important than other because determinate some agreement as COP21 in Paris (2015). In this conference it was decided to try to limit global warming by taking under 2°C of increase, doing whatever it takes to get under 1.5°C. [6]

It was one of the largest agreements in history as was the Kyoto Protocol in 1997, but the main difference lies in the way in which the goal can be achieved, which is decided independently by each country. Some nations focus on reduction of CO₂ emissions, other looking at other parameter as energy intensity (especially developing nations like China and India).

Looking at our part of World, the European Union decided to focus themselves to the following parameters:

1. Reduction of 55% of GHG (greenhouse gases) emissions compared to level of 1990.
2. At least 32% share for renewable energy.
3. At least 32.5% improvement in energy efficiency. [6]

This is a controversial argument because someone appreciates the effort of European Commission instead other people criticize the lack of bravery, firmly believing that it is possible to do better.

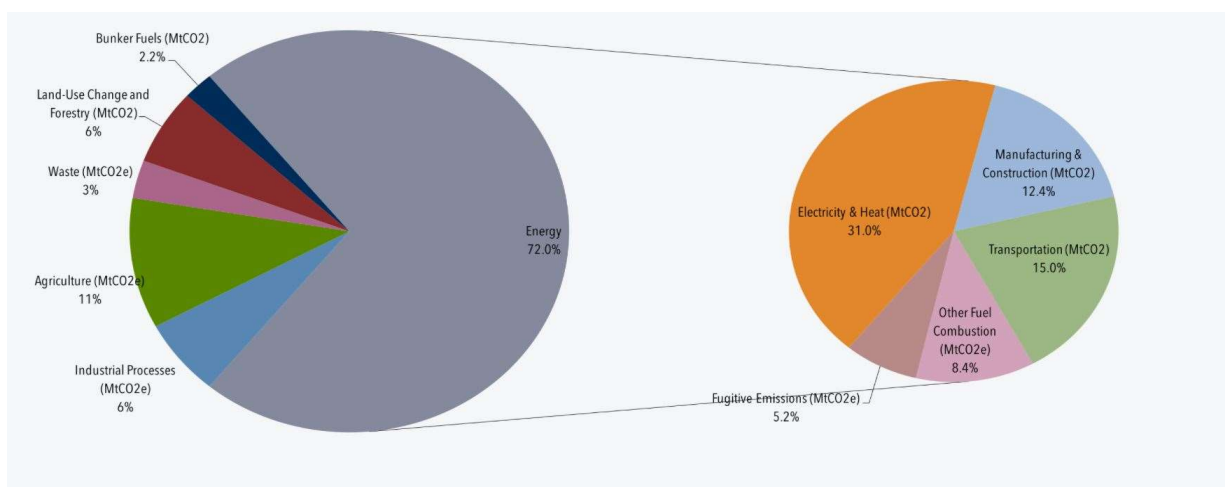


Figure 2 - CO₂ emissions by source [8]

This contextualisation is useful to appreciate the global context in which our technology can play or not a role inside global market. According to the BBC, in 2018 transport sector was responsible of a quarter of total CO_2 emissions in UK (2018) [7] but some other studies resize this percentage globally around 11%. [8] I consider this value as more realistic one due to small reduction of global emissions, around 5.8% according to the International Energy Agency, despite global pandemic of 2020 that drastically reduced for at least 5/6 months global transport sector. [9]

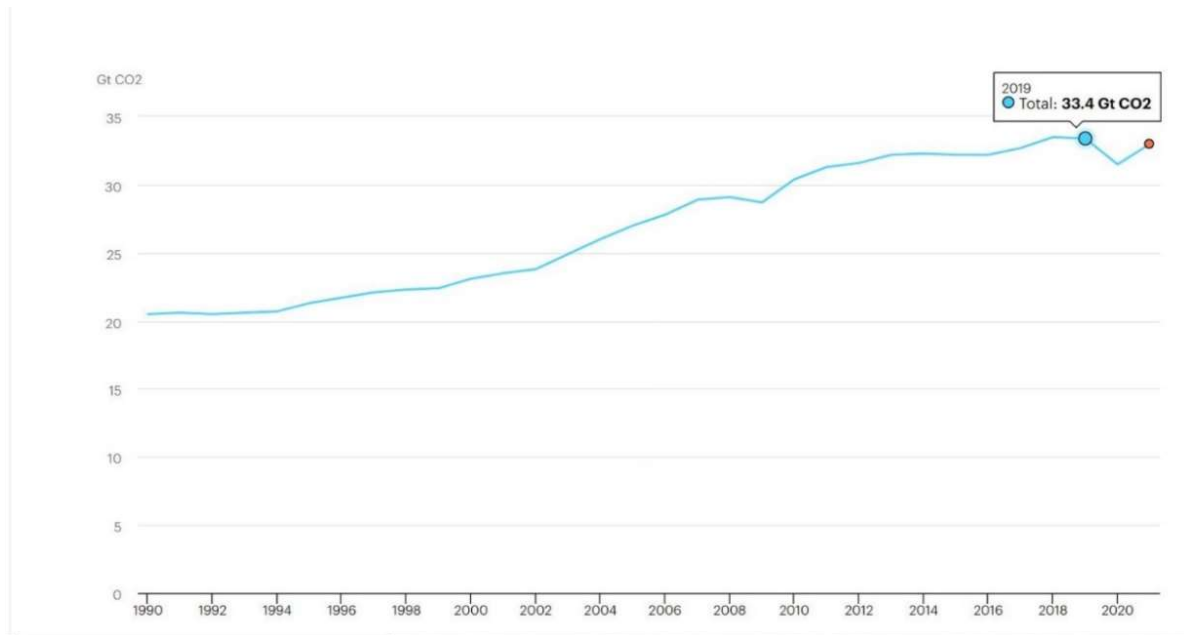


Figure 3 - Global CO_2 emissions by year [9]

Obviously, this reduction is not only caused from the stop of transport sector, but the use of cars, buses or trains is certainly one of the most affected sectors during the various lockdowns.

The reason why we take lot of care of this sector is twofold:

1. 11% of global emissions mean around 3.7 Gt of CO_2 looking at the peak of 2018 (33.5 Gt) that is not negligible amount.
2. Transport sector is strictly related to other sectors, reducing its impact can delay or reduce some not sustainable processes as, for example, extraction and transport of oil.

Today transport sector is moving from oil to electricity, most of automotive companies today produce at least an electrically or hybrid motorized car but there are still some huge problems in electrical vehicle. Electrical cars use ion lithium battery that have huge degradation that determinate an increase of internal resistance (RI) and loss of electrolyte (LE) caused by some internal physical or chemical side reactions. These kinds of phenomena take a relevant role when temperature increase, reducing consistently the number of cycle possible for batteries. [10] The two most relevant issues are related to the mining of lithium and to the recycle of battery. Lithium can be extract from mining process as it happens in Africa or through the evaporation of salad groundwater (Chile) but the huge increase in extraction is not sustainable, in fact someone talks about an increase of 10 times the actual rate in 10 years. The recycle of battery is difficult too because the production of this type of batteries consists in the overlapping

of layers that are pressed together at high temperatures thus preventing easy separation during the recycling phase.

Fuel cells have not this kind of problem because they don't need huge accumulation of energy but there are still problems with the use of precious metals for the catalyst (such as platinum), which increases costs and complicates supply.

Today there are some interesting applications of FCs in automotive sector as for example Toyota Mirai and Hyundai Nexa and all this application use PEMFCs because they can work at low temperature allowing their use instantaneously without start-up time preparation.

Autonomy of hydrogen cars is one of the main strengths, in fact each one can reach 650 km with tank full of hydrogen and time of tank recharge are around five minutes compared to some hours of charge of electric battery. Main limitations are the lack of recharge points and cost of fuel cells but an increase in recharging points combined with a decrease in the price of cars could give a boost to the sector and encourage a greater diffusion of this type of cars and a consequent demand for new recharging points, triggering a virtuous motion. The lack of recharge points can be filled with public investment that can finance this sector priming this chain reaction.

1.3 State of art in automotive sector

The attentions of automotive companies for new power technologies are growing fast, and not only for battery electric vehicle but also for hydrogen model, for example, BMW is testing its prototype called “BMW i Hydrogen Next” [11] due to evaluate reliability, safety and efficiency. However, today there are already some interesting FCs vehicle models on the market as:

- Toyota Mirai
- Hyundai Nexa
- Honda Clarity

The growing attention for this technology is also highlighted by the last year announcement of PSA group for a new FC van and furthermore Audi is thinking about a small series of luxury FC SUV by 2023[12]. However, Toyota Mirai is certainly the current landmark because the 2020 version is the third revision of Fuel cells for Toyota (2008/2014) and the improvements are significant as it’s reported in table 1.

	TOYOTA PEMFCs		
	2008 VERSION	2014 VERSION	2020 VERSION
CRUISE RANGE [km]	330	500	650
RECHARGING TIME [min]	8	5	5
MAXIMUM POWER [kW]	90	114	128
POWER DENSITY [kW/kg]	0,83	2	4,4
THICKNESS OF CELL [mm]	1,68	1,34	1,1
NUMBER OF CELLS	400	370	330
EXTERNAL CIRCULATING HUMIDIFIER	YES	YES	NOT PRESENT

Table 1 - Toyota FCs comparison [11][13][14][15]

The main efforts are aimed at improving all those characteristics that would make the car conform to its traditionally powered equivalents. For this reason, efforts are directed towards reducing dimensions and weight of fuel cells, parameters that directly affect the power density, the efficiency of cell but also the comfort and performance of the car.

There are also some applications for Fuel Cell Electric Bus (FCEB) with first 600 vehicles available in Europe in Denmark, Latvia and UK and maintenance cost around 0.25 to 0.35 €/km [12].

1.4. Polarization Curve

Main targets for automotive companies are to create a new powered vehicle which can be replaceable to the actuals on the market. So big efforts will be direct on increase of power and durability, reduction of cost but keeping high level of cruise range. To increase power, is useful to introduce one of the main concepts: the polarization curves.

The polarization curve is a graph obtained from the cell behaviour in its voltage and current characteristic and it's measured experimentally. In figure 4 it's shown a typical example with typical losses:

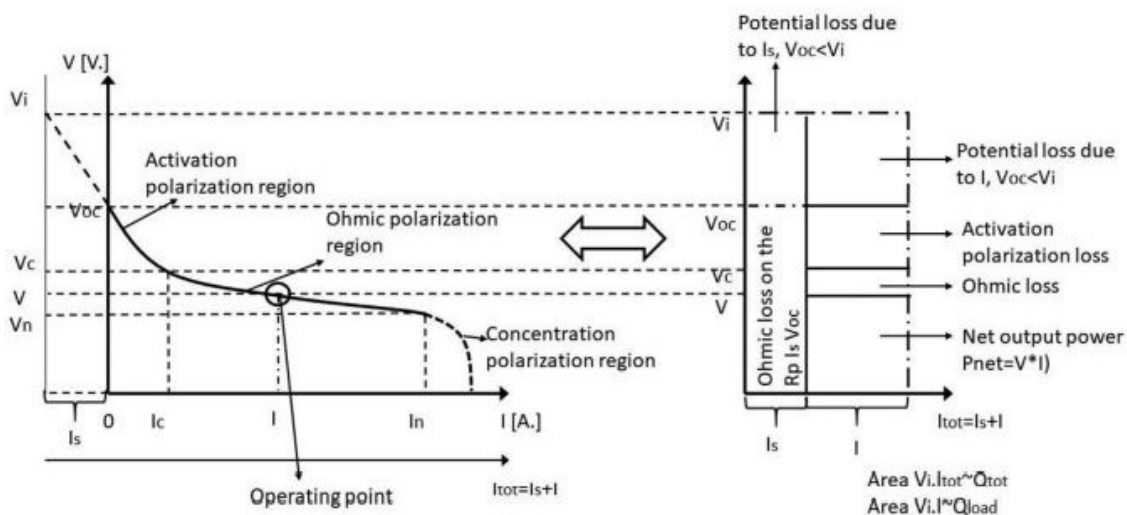


Figure 4 - Typical FC polarization curve [16]

Each type of fuel cell presents his own polarization curve but there are three main regions we can always distinguish:

1. Activation region;
2. Ohmic region;
3. Concentration polarization regions.

The activation region is obtained at the beginning of the test in no load case and in this zone voltage drops exponentially; it decreases until the value of voltage called V_c where it starts the region and where Ohmic losses dominate the process. Each chemical reaction requires an amount of energy to start and the energy losses in activation zone are related to the energy the reaction needs to start. After this region we have linear losses and they depend on serial resistance R_s . The last zone is reached for high value of current where it's possible have some damages of FC because there is a fast voltage drop.[16]

The analytic evaluation of this curve is presented very well in the paper of Chen [17]:

$$E(t) = E_{rev} - E_{act,a}(t) - E_{act,c}(t) - E_{ohm}(t) - E_{conc,a}(t) - E_{conc,c}(t)$$

This equation puts in relation how voltage changes in time. In no load conditions, we have the maximum value of Voltage (E_{rev}) called reversible voltage

$$E_{rev} = E_{rev}^0 + \frac{RT}{kF} * \ln \left(\frac{P_{H_2} P_{O_2}^{0.5}}{P_{H_2O}} \right)$$

E_{rev}^0 is reversible Nernst voltage and pressure values are referred to partial pressures of gases in the mixture.

For the activation region and for the concentration polarization region we evaluate losses separately for cathode and anode. For activation region at the anode side, we use the equation below:

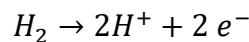
$$E_{act,a}(t) = \frac{RT}{2\alpha_a F} * \ln \left(\frac{J_{loss(t)} + \frac{I(t)}{A(t)}}{J_{0,a}} \right)$$

An analogue equation is used for the cathode side:

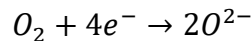
$$E_{act,c}(t) = \frac{RT}{4\alpha_c F} * \ln \left(\frac{J_{loss(t)} + \frac{I(t)}{A(t)}}{J_{0,c}} \right)$$

○ α is the charge coefficient and it affects the reaction mechanism. It represents the amount of interfacial potential in the electrode-electrolyte interface.

○ $J_{loss(t)}$ is time dependent and it's the current density lost while $J_{0,a}$ and $J_{0,c}$ are the exchange current densities at each electrode. At the anode we have the number of free electrons equal to 2 due to hydrogen oxidation:



At the cathode side the number of free electrons is 4 due to oxygen reduction:



Concentration losses can be neglected at the anode side because hydrogen diffusion is bigger in nitrogen than oxygen, therefore we have only concentration loss at the cathode:

$$E_{conc,c}(t) = B_{c(t)} \cdot \ln \left(1 - \frac{I(t) * A(t)}{J_{max,c(t)}} \right)$$

- $B_{c(t)}$ is the water and gas accumulation coefficient;
- $J_{max,c(t)}$ is the current density limit at the cathode.

The polarization curve is related always to a singular type of cell and it's influenced by a great number of factors: typology of cell, catalyst, catalyst deposition and others.

It's directly related to physical conditions: as it will be presented in the following chapters, for each type of cell there can be a huge number of polarization curves. The differences arise from temperature difference and humidity conditions. They directly influence the behaviour of the membranes and consequently the cell's performances. For these reasons if energy industry wants to see an increase of power, it is crucial to improve polarization curve, to limit losses, and to extend the maximum usable voltage.

1.5. *Future development*

Improving main parameters of PEMFCs is essential to make FCs vehicles competitive with traditional ones. The main efforts are planning to reduce the use of Platinum, to improve maximum power and cell durability but looking at overall cost reduction. In table below (table 2) is shown the actual result and the target to make possible a massive usage of this technology in automotive sector.

	CURRENT DENSITY [A/cm²]	VOLTAGE REFERENCE [V]	POWER DENSITY [kW/l]	OPERATING TEMPERATURE [°C]	PLATINUM LOADING [g/kW]
2020 VERSION	2,6	0,6	5,38	90	0,1-0,2
2024 TARGET	4-5	0,8-0,9	9	100	<0,1

Table 2 - new PEMFCs target [14]

I want to highlight that these targets are ambitious in a relatively small amount of time for research. One of the main aspects of research is the catalyst layer: the target suggests platinum should reduce but performances should increase. It seems nonsense but it's not because catalyst deposition is one of the main working aspects to improve cell performances. It's a crucial aspect due to the optimization of catalyst surface, in fact increasing platinum reagent surface allows to improve performance with the same amount of substance. An example is reported in the same paper, where it is suggested the use of Pt_3Ni that can achieve enhancement factor of 22 in specific activity compared to commercial Pt/C catalyst.[14]

1.6. Catalyst deposition

Catalyst ink is usually deposited with the purpose of reaching a homogenisation between catalyst and electrolytic membrane (figure 5), during this work it will be presented an example from laboratory of Politecnico of Turin.

As is reported at the beginning of this thesis, there are different ways to deposit catalyst inks: magnetic stirring, high-shear mixing, ball-milling (also called bead milling) hydrodynamic cavitation or by acoustic cavitation (ultrasonic agitation).[3]

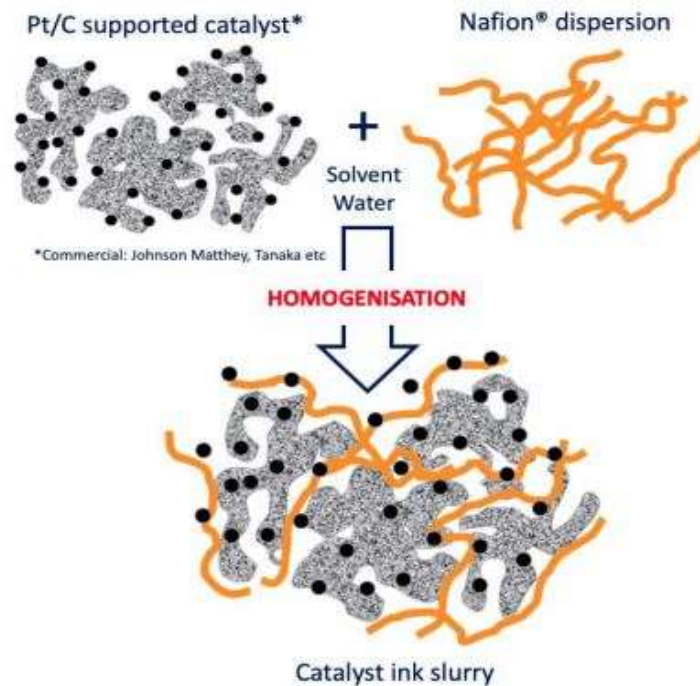


Figure 5 – Catalyst deposition [3]

Today the most used techniques are the following:

- Ultrasound is the traditional method; it consists in the mixing of catalyst inks and electrolytic membrane in pure water through ultrasonic exposure at variable level of frequency and time (usually 20-40 kHz and up to 15 minutes to 3 hours).[3]
- Ball-milling (bead milling) is a procedure that provide a mixing process between a liquid mixture of catalyst inks with electrolytic membrane and ceramic or metal balls. The collisions created by this method generate the dispersion of ink. [18]
- Hydrodynamic cavitation is a process that produces cavitation bubble more efficiently than ultrasonic method. It has some advantages than previous described methods because this procedure results provide minimal damages and high productivity.[18]

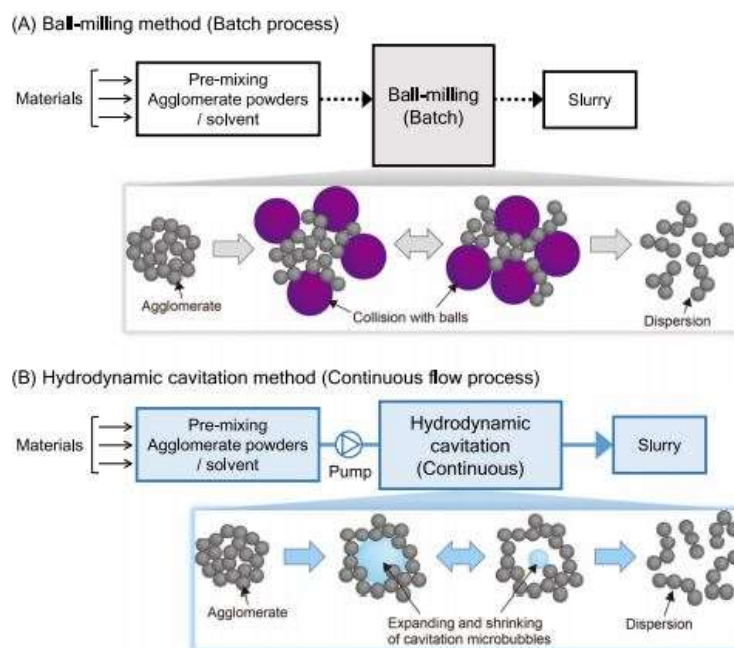


Figure 6 - Ball milling and hydrodynamic cavitation [18]

In Figure 6 is presented how physically works ball milling method and hydrodynamic cavitation, and how the catalyst agglomerate can be expanded and dispersed to increase the reactant surface.

As it's explained before, catalyst is crucial point in fuel cell development because it is one of the most expensive part of process and reducing the use of platinum may means big steps forward for the industrialization of PEMFC technology. Indeed, if it were possible to use less platinum having the same performance it would be obvious a convergence of all FC producers into the most convenient method. Catalysts are required to decrease the activation energy but activation energy decreases also when temperature increase. For this reason, researchers are searching for the right compromise that can allow to increase temperature in order to decrease the amount of platinum, avoiding water boiling point.

I close this introduction chapter with figure 7, where it is presented the result of experimental study held by H. Kuroki, K. Onishi in which it is shown that ball-milling and hydrodynamic cavitation present similar results so it is difficult to define properly which methods guarantee better results. For this reason, other factors become crucial for the choice as for example electrical results or costs of processes.

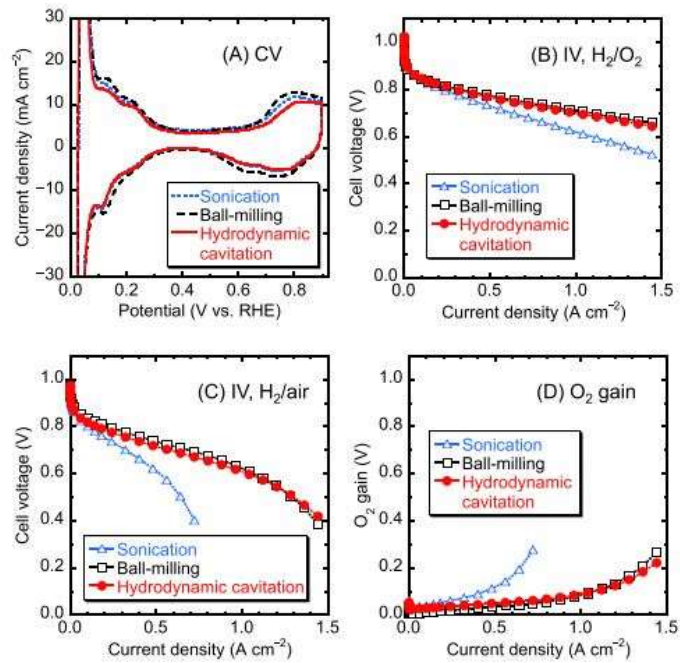


Figure 7 - Catalyst deposition comparison

The main emerging aspect in figure 7 is the sonication of catalyst ink is not performing as the other two methods and, analysing only the efficiency point of view, the experimental results suggest avoiding this solution and to focus on the other two, working on lowering process cost and increase in performances.

2. Model explanation

To analyse and to compare the characteristics of FCs the scientific community requires some standardization parameters and standard model codes useful to compare results and to avoid each researcher should create one personally. A group of researchers guided by Vetter and Schumacher create a new code and they give it for free at the following link:

<http://dx.doi.org/10.17632/2msdd4j84c.1> [19]

2.1. How does it work?

The model is based on MATLAB simulation, it provides five different layers to represent in 1D model the Membrane electrode assembly (MEA). Central layer is the proton exchange membrane (PEM) that is between two catalyst layers (CLs) and the external layers are the gas diffusion layers (GDLs). At the end it considers bipolar plates as boundaries of the MEA. [19] The graphical model representation is provided in figure 8.

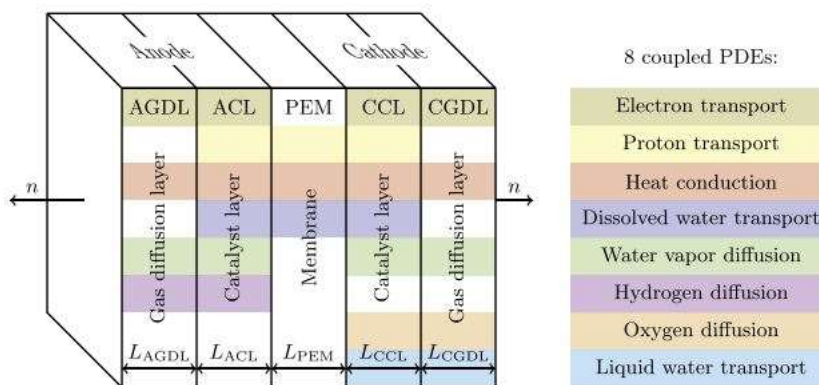


Figure 8 – MATLAB model representation [19]

On the right-hand side of figure 8, there are 8 partial differential equations (PDE) used in model:

- *The electron and proton transport equations* are governed by Ohm Law in catalyst layers and in gas diffusion layers.
- *The heat conduction equation* is the third one and it is related to Fourier law.
- *Dissolved water transport* is governed by Springer equation and it regulates water balance.
- *Gas diffusion equations* are governed by Fick's transport model and are split in three different equations: hydrogen diffusion at the anode side, oxygen diffusion at the cathode side and water vapor diffusion for each side.
- *Liquid water transport* is obtained adapting Darcy law thanks to the water saturation gradient.[19]

The proposed model is updated based on the model developed by Monteverde et al. [<https://iopscience.iop.org/article/10.1149/MA2020-02332095mtgabs/meta>] where the proposed equations are resolved through COMSOL.

2.2. Analytical explanation

The complexity of this model is related to the number of equations that are required to explain the physical processes relations, how all parameters interact each other and how these interactions influence experimental result. There are some main categories to consider:

1. Electrochemistry equations.
2. Heat/mass transport equations.
3. Phase transitions equations.
4. Boundaries conditions.

2.2.1. Electrochemistry equations

The starting point of model analysis is certainly electrochemistry. The Nernst equation determines the maximum voltage available for each cell and it's the maximum voltage physically reachable:

$$\Delta\Phi = -\frac{\Delta G}{2F} + \frac{RT}{4F} * \ln \left[-\frac{P_{H2}}{P_{ref}} * \left(\frac{P_{O2}}{P_{ref}} \right)^{0.5} \right]$$

Where:

- ΔG is Gibbs free energy $\left[\frac{J}{mol} \right]$;
- F is the Faraday constant and it is equal to $96485 \left[\frac{C}{mol} \right]$;
- R is gas constant $\left[\frac{J}{mol K} \right]$;
- T is temperature $[K]$;
- P represents the partial pressure of the gas in subscript $[Pa]$.

The model needs to consider the cell overpotential that is the difference between the potential at standard conditions and the potential at the considered conditions.

The reversible potential difference evaluation is made by looking at the following equations:

$$\Delta\Phi_0 = -\frac{T*\Delta S}{2F} - \frac{RT}{2F} * \ln \left[\frac{P_{H2}}{P_{ref}} \right] \text{ in anode catalyst layer;}$$

$$\Delta\Phi_0 = -\frac{\Delta H - T*\Delta S}{2F} + \frac{RT}{4F} * \ln \left[\frac{P_{O2}}{P_{ref}} \right] \text{ in cathode catalyst layer.}$$

2.2.2. Heat/mass transport equations

Heat and mass transport phenomena are evaluated with 8 differential equations useful to provide a complete description of how ions interact inside the cell. The explanation is previously reported but now I want to evaluate the analytical terms of each one:

The electron and proton transport equations are governed by Ohm Law:

$$\begin{aligned}j_e &= -\sigma_e * \nabla \Phi_e \\j_p &= -\sigma_p * \nabla \Phi_p\end{aligned}$$

Where:

- j_e is the flux of electron $\left[\frac{A}{m^2}\right]$;
- j_p is the flux of proton $\left[\frac{A}{m^2}\right]$;
- σ is the electric conductivity $\left[\frac{S}{m}\right]$;
- Φ is the electronic phase potential [V]; [19]

The heat conduction equation is related to Fourier law.

$$j_T = -k * \nabla T$$

Where:

- j_T is the heat flux $\left[\frac{W}{m^2}\right]$;
- k is thermal conductivity $\left[\frac{W}{m K}\right]$;
- T is temperature [K]. [19]

Dissolved water transport into ionomer is governed by Springer equation.

$$j_\lambda = -\left(\frac{D_\lambda}{V_m}\right) * \nabla \lambda + \left(\frac{\xi}{F}\right) * j_p$$

Where:

- j_λ is the molar flux of dissolved water $\left[\frac{mol}{m^2 s}\right]$;
- D_λ is the effective diffusion coefficient with respect to water content gradient $\left[\frac{m^2}{s}\right]$;
- $\nabla \lambda$ is the ionomer water gradient [-];
- F is the Faraday constant and it is equal to 96485 $\left[\frac{C}{mol}\right]$;
- ξ is the electroosmotic drag coefficient [-]. [20]

Gas diffusion equations are governed by Fick's transport.

Fickian Diffusion Coefficient Expressions are useful to describe the diffusion of gases in presence of gradient of concentration. The expressions are:

$$\begin{aligned}j_{H_2O} &= -C * D_{H_2O} * \nabla X_{H_2O} \\j_{H_2} &= -C * D_{H_2} * \nabla X_{H_2} \\j_{O_2} &= -C * D_{O_2} * \nabla X_{O_2}\end{aligned}$$

Where:

- j is diffusion flux for each gas $\left[\frac{mol}{s}\right]$;
- C is the interstitial gas concentration $\left[\frac{mol}{m^3}\right]$;
- D is diffusion coefficient $\left[\frac{m^2}{s}\right]$;
- x is the position $\left[\frac{mol}{s}\right]$. [19]

Liquid water transport is obtained adapting Darcy law

$$j_s = -\frac{k}{\mu * V_W} * \frac{\delta p}{\delta s} * \nabla s$$

Where:

- j_s is liquid water flux $\left[\frac{mol}{m \cdot K}\right]$;
- k is the hydraulic permeability $\left[\frac{W}{m \cdot K}\right]$;
- μ is the dynamic viscosity of liquid water $[Pa \cdot s]$;
- V_W is the volume of water $\left[\frac{m^3}{mol}\right]$;
- s is the liquid water saturation $[-]$;
- δp is the capillary pressure $[Pa]$. [19]

To solve differential equations, initial and boundary conditions are required and they are setting looking at physical behaviour of cell. For each layer boundary are imposed 2 boundary conditions for every differential equation.[19]

2.2.3. Phase transitions equations.

A crucial role is taken by the change of water phase, an aspect that must be observed with lot of attention to limit possible damages or excessive water content. Water management is fundamental aspect to ensure not only the perfect working condition but mainly to avoid future decrease in lifecycle of PEMFCs.

The model has to consider every heat generation source and in order to do it the first term is the water split reaction. It provides two different sorption terms S_e e S_p related to electron and proton.

The second term considered by the model is the water adsorption term:

$$S_{ad} = \frac{k_a}{L V_m} * (\lambda_{eq} - \lambda)$$

Where:

- k is mass transfer coefficient and it depends on material. $[\frac{m}{s}]$;
- L is the catalyst layer thickness $[m]$;
- V_m is the molar charge ionomer volume $[\frac{m^3}{mol}]$. [19]

The third heat source is related to evaporation and condensation terms and the model evaluates this term as:

$$S_{ec} = \gamma_{e/c} * C * (x_{H2O} - x_{sat})$$

Where:

- S_{ec} evaporation or condensation source $[\frac{mol}{m^3*s}]$;
- γ is the evaporation (e) or condensation (c) rate $[\frac{1}{s}]$;
- C is the total interstitial gas concentration $[\frac{mol}{m^3}]$;
- x_{H2O} is water vapor mole fraction $[-]$;
- x_{sat} is saturation water vapor mole fraction $[-]$. [19]

This part of model is completed adding the contribution of latent heat during phase transitions ($S_{T,ad}$, $S_{T,ec}$) and other heat source related to electric and ionic currents ($S_{T,e}$, $S_{T,p}$) and the waste heat of electrochemical reactions. ($S_{T,r}$).

All the heat terms are summarized in the table below (Table 3) [19]:

S_e	Electron reaction rate $[\frac{A}{m^3}]$	$S_{T,ec}$	Evaporation/condensation heat source $[\frac{W}{m^3}]$
S_p	Proton reaction rate $[\frac{A}{m^3}]$	$S_{T,e}$	Joule heat source of electrons $[\frac{W}{m^3}]$
S_{ad}	Water absorption source $[\frac{mol}{m^3 s}]$	$S_{T,p}$	Joule heat source of protons $[\frac{W}{m^3}]$
S_{ec}	Evaporation/condensation source $[\frac{mol}{m^3 s}]$	$S_{T,r}$	Reaction heat source $[\frac{W}{m^3}]$
$S_{T,ad}$	Water ab-/desorption heat source $[\frac{W}{m^3}]$		

Table 3- Heat source generation summarize

2.2.4. Parametrization

The model is useful to compare different typologies of membranes and it is able to provide the main cell parameters. Different equations are used to parametrize:

- Water properties.
- Electrochemical parameters.
- Ionomer parameters.
- Transport parameters.

From the point of view of water properties, the first parameter is the saturation pressure and it is evaluated with the **Antoine Equation**. It describes the relation between saturation pressure and temperature with the following relation:

$$P_{sat} = e^{A + \frac{B}{C-T}}$$

Where:

- P_{sat} is saturation pressure [Pa];
- A [-], B [K], C [K], are liquid characteristic coefficients, evaluated experimentally;
- T is temperature [K].

To evaluate water dynamic viscosity the model use **Vogel Equation**:

$$\mu = e^{A + \frac{B}{T-T_0}}$$

Where:

- μ is water dynamic viscosity [mPa*s];
- A , B [K], T_0 [K] are constant;
- T is the absolute temperature [K].

Another important equation to consider is certainly the one able to show how current is a function of the particles concentration and temperature, and the equation was evaluated by Butler-Volmer [19]:

$$i_0 = 0.27 * e^{\frac{16}{R} * \left(\frac{1}{T_{ref}} - \frac{1}{T} \right)}$$

Where:

- i_0 is exchange current density [$\frac{A}{cm^2}$];
- R is gas constant [$\frac{J}{mol K}$];

- T_{ref} is the reference temperature (353K);
- T is the temperature [K] [19].

In the previous equation, the factor 0.27 is measured in $\frac{A}{cm^2_{Pt}}$ and the amount of platinum surface area changes for cathode and anode side: active surface area density is equal to $1 * 10^{11} \frac{cm^2_{Pt}}{m^3}$ for the anode catalyst layer and $3 * 10^{11} \frac{cm^2_{Pt}}{m^3}$ for cathode catalyst layer. The symmetry factor or the half-reactions is 0.5 in this case. [19]

2.2.5. Principal ionomers parameters

There are some parameters that are directly influenced by ionomer's characteristic.

The first parameter modelled through an equation, validated for the Nafion membranes, is the ionic conductivity whose behaviour is parameterised through the Arrhenius expression to describe the real experimental trend.

$$\sigma_p = k * e^{\frac{15}{R} * \left(\frac{1}{T_{ref}} - \frac{1}{T} \right)}$$

Where:

- σ_p is the ionic conductivity of proton [S/m];
- k is the constant experimentally evaluated.
- R is gas constant $\left[\frac{kJ}{mol K} \right]$;
- T_{ref} is the reference temperature (353K);
- T is the temperature [K]. [19][21]

In this condition the parameter sets to 15 [kJ/mol] is the energy activation.

The equation behind the diffusivity ionomer parameter was studied to Mittelstaedt and Staser: looking at the experimental results, they evaluated a complex equation based on complex rational polynomial that can be easily resume as:

$$D_\lambda = f(\lambda) * e^{\frac{20}{R} * \left(\frac{1}{T_{ref}} - \frac{1}{T} \right)}$$

Where:

- D_λ is the diffusion coefficient of dissolved water $\left[\frac{m^2}{s} \right]$;
- λ is the ionomer water content [-];
- R is gas constant $\left[\frac{J}{mol K} \right]$;
- T_{ref} is the reference temperature (353K);
- T is the temperature [K]. [19]

One of the last fundamental parameters is the ionomer water content that can be calculated with the equation reported below:

$$\lambda_{eq} = 0.043 + 17.81 * RH - 39.85 * RH^2 + 36.0 * RH^3$$

Where:

- λ is the ionomer water content [-];
- RH is the relative humidity at current collectors [-].

The next-to-last parameter involved is the mass transfer coefficient of vapour related to Nafion membranes and it includes the absorption of water from a gas diffusion layer/ membrane interface, the water transport through the membrane and desorption processes in another GDL/membrane interface [22]:

$$k_{a,d} = a_{a,d} * e^{\frac{20}{R} * \left(\frac{1}{T_{ref}} - \frac{1}{T} \right)}$$

Where:

- $k_{a,d}$ is water absorption or desorption transfer coefficient $\left[\frac{m}{s} \right]$ [12];
- $a_{a,d}$ is a constant of absorption or desorption transfer coefficient $\left[\frac{m}{s} \right]$;
- R is gas constant $\left[\frac{J}{mol K} \right]$;
- T_{ref} is the reference temperature (353K);
- T is the temperature [K] [19].

The last important parameter is the water diffusivity estimated with Chapman-Enskog formula:

$$D_x = \frac{\epsilon_p}{\tau^2} (1 - s)^3 D_{x,ref} \frac{T}{T_{ref}} \frac{P_{ref}}{P}$$

Where:

- D_x Fickian diffusion coefficient of gas X $\left[\frac{m}{s} \right]$;
- ϵ_p porosity volume fraction [-];
- τ pore tortuosity [-];
- s is the liquid water saturation [-];
- $D_{x,ref}$ is the diffusivity of X at reference conditions $\frac{m^2}{s}$. [19]

3. Reference model evaluation

Looking at the literature used before [19] there are some interesting data available, useful to explain in detail how analytic model on COMSOL works. Starting from the aim to demonstrate the validity of the proposed model is useful to look at current data available in literature.

The data reported below are available as an example of the paper propose previously. The purpose is to demonstrate that starting from the same data, the same results are obtained. To do that, the table below (table 4) shows different tests performed at different temperature, pressure and moisture conditions. In this work, for each test, it will be proposed the main results and obviously the evaluation of current and voltage profile for each stage of interest.

	Temperature at current collectors T _c [°C]	Anode absolute Pressure P _{a(a)} [bar]	Cathode absolute Pressure P _{c(a)} [bar]	Relative humidity at current collectors RH [%]	Liquid water saturation at cathode current collector s _c
TEST T0	80	2,5	2,3	40	0
TEST T1	45	2,5	2,3	85	0,12
TEST T2	95	2,5	2,3	22,5	0,12
TEST T3	95	2,5	2,3	35	0
TEST T5	95	2,5	2,3	47,5	0
TEST T6	95	1,6	1,4	40	0
TEST T7	95	3	2,8	40	0

Table 4- Starting data for model evaluation

In table 4 the common parameters are reported but there are a huge number of other parameters in common for each test. These parameters are divided into:

- General parameters.
- Geometrical parameters.
- Current distribution parameters.
- Ionomer end water parameters.
- Thermal parameters.
- Gas diffusion parameters.

The table below (table 5) shows how many parameters are behind the model and so how complex can be the analysis of problem. This is the reason why in the following chapter I will simulate just a very little part of the problem, trying to understand better how temperature working conditions influence electrolytical membrane performance.

General parameters		Geometrical parameters		Current Distribution Parameters	
Reference pressure [p_ref]	1.0133E5 Pa	GDL thickness [L_gdl]	160[um]	Electric conductivity, GDL [sigma_s_gdl]	1250[S/m]
Water partial pressure at current collectors [p_H2O_cc]	18947 Pa	Catalyst layer thickness [L_cl]	10[um]	Electric conductivity, catalyst layer [sigma_s_cl]	350[S/m]
Oxygen partial pressure at cathode current collector [p_O2_cc]	44321 Pa	Membrane thickness [L_pem]	25[um]	Reference exchange current density, oxygen reduction [iO_orr_ref]	2.45e-8[A/cm^2]
Hydrogen partial pressure at anode current collector [p_H2_cc]	2.3105E5 Pa	Ionomer volume fraction, catalyst layer [eps_l_cl]	0.3	Reference exchange current density, hydrogen oxidation [iO_hor_ref]	0.27[A/cm^2]
Reference temperature [T_ref]	353.15 K	Gas pore volume fraction, catalyst layer [eps_p_cl]	0.4	Specific surface area, anode [A_a]	1e11[cm^2/m^3]
Oxygen partial pressure, initial value [p_O2_init]	44321 Pa	Gas pore volume fraction, GDL [eps_p_gdl]	0.76	Specific surface area, cathode [A_c]	3e11[cm^2/m^3]
Hydrogen partial pressure, initial value [p_H2_init]	2.3105E5 Pa	Tortuosity [tort]	1.6	Entropy change, oxygen reduction [delta_S_orr]	-163.3[J/mol/K]
Temperature, initial value [T_init]	353.15 K			Entropy change, hydrogen oxidation [delta_S_hor]	0.104[J/mol/K]
Water partial pressure, initial value [p_H2O_init]	18947 Pa			Enthalpy change [delta_H]	-285.83[kJ/mol]
Liquid water saturation at cathode current collector [s_c]	0			Initial equilibrium potential, hydrogen oxidation [Eeq_hor_init]	-0.012733 V
Ionomer and water Parameters					
Acid equivalent volume of membrane [Vm]	5.1777E-4 [m^3/mol]	Water absorption transfer coefficient prefactor, catalyst layer [k_abs_cl]	1E-13 [m^2]	Initial equilibrium potential, oxygen reduction [Eeq_orr_init]	1.1761 V
Liquid-gas interfacial area density prefactor [A_gl]	2E6 [1/m]	Molar volume of liquid water [Vw]	1.8405E-5 [m^3/mol]	Initial cell equilibrium voltage [Eeq_cell_init]	1.1888 V
Water absorption transfer coefficient prefactor, GDL [k_abs_gdl]	6.15E-12 [m^2]	Water molar weight [Mw]	0.018 [kg/mol]	Operating cell voltage [E_cell]	1 V
Thermal parameters				Gas diffusion parameters	
Thermal conductivity, GDL [kappa_gdl]	1.6[W/(m*K)]	Activation energy, oxygen reduction [Ea_orr]	67[kJ/mol]	Reference oxygen diffusivity in cathode gas mixture [D_O2_ref]	0.28[cm^2/s]
Thermal conductivity, catalyst layer [kappa_cl]	0.27[W/(m*K)]	Activation energy, hydrogen oxidation [Ea_hor]	16[kJ/mol]	Reference hydrogen diffusivity in anode gas mixture [D_H2_ref]	1.24[cm^2/s]
Thermal conductivity, membrane [kappa_pem]	0.3[W/(m*K)]	Activation energy, ionomer conductivity [Ea_sigma]	15[kJ/mol]	Reference water diffusivity in anode gas mixture [D_H2O_A_ref]	1.24[cm^2/s]
Heat of evaporation-condensation [H_ec]	42[kJ/mol]	Activation energy, water diffusion in ionomer [Ea_lambda]	20[kJ/mol]	Reference water diffusivity in cathode gas mixture [D_H2O_C_ref]	0.36[cm^2/s]
Heat of water adsorption [H_ad]	H_ec	Activation energy, water adsorption [Ea_ad]	20[kJ/mol]		

Table 5 – Common test parameters

The next step of the procedure is the evaluation of the model: the model on COMSOL provides a huge number of curves related to the physical parameter that influences the process. Some of the most important curves are the polarization and power curves and some examples are reported in the next page (figure 9).

They look very similar one to another and for this reason I selected one of them to present a characteristically polarization curve, in this case for test T1.

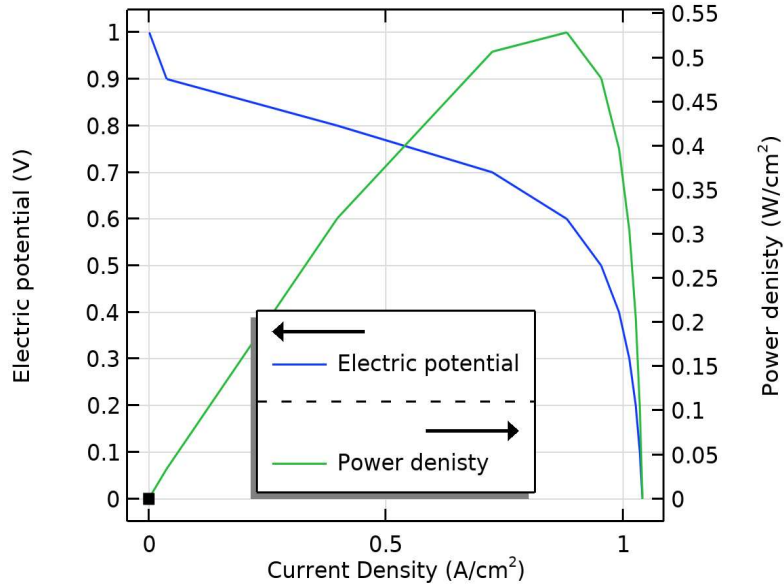


Figure 9 - Test condition T1

Even small improvements in the polarization curve could be crucial for research because each progress could mean a decrease of use of precious catalyst or a performance increasing. The membranes electrode assembly (MEA) is repeated a certain number of times to increase performance and achieve the desired power. For this reason, each small advance becomes significant as the single unit is repeated on a large scale and this promotes its commercialisation.

To validate the model, I provide the reference numbers available in the paper comparing them with the output number of COMSOL model in the same working points, estimating the error too.

	T0			T1			T2			T3		
	REFERENCE	MODEL	ERROR									
U[V] at 0.1 A/cm ²	0,829	0,848	-0,019	0,863	0,884	-0,021	0,789	0,803	-0,014	0,822	0,851	-0,029
U [V] at 0.8 A/cm ²	0,412	0,417	-0,005	0,661	0,652	0,009	0,000	0,000	0,000	0,435	0,490	-0,055
I [A/cm ²] at 0.4V	0,809	0,815	-0,006	0,991	0,992	-0,001	0,556	0,565	-0,009	0,842	0,922	-0,080
Maximum cell power [W/cm ²]	0,367			0,529			0,238			0,393		
	T5			T6			T7					
	REFERENCE	MODEL	ERROR									
U[V] at 0.1 A/cm ²	0,848	0,866	-0,018	0,816	0,825	-0,009	0,834	0,857	-0,023			
U [V] at 0.8 A/cm ²	0,605	0,609	-0,004	0,359	0,349	0,010	0,435	0,447	-0,012			
I [A/cm ²] at 0.4V	1,137	1,141	-0,004	0,770	0,772	-0,002	0,826	0,836	-0,010			
Maximum cell power [W/cm ²]	0,511			0,340			0,379					

Table 6- Paper and model data comparison

At first, it is useful to compare if the model returns the same output declared by the paper's authors in the working point declared. Looking at the data, there are a correlation that show similar results and this is the first crucial consideration to do with the aim to keep the following

results as acceptable. In second order is useful to evaluate what kind of conditions gives us maximum power, as it can be observed in the last line of table 7.

The maximum cell power is returned by the test number 1 that is performed at lowest temperature and higher level of moisture. It's not surprising that the test at higher level of moisture give back that kind of results because the right cell humidification allows better results in term of water molecules transition.

To demonstrate the validation of the model, in figure 10 and figure 11 are reported the graphs comparison for respectively test T1 and test T3

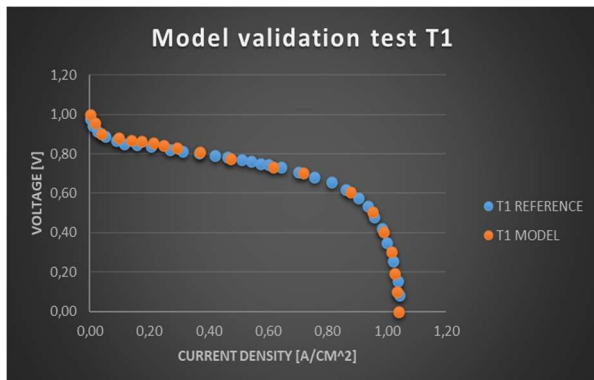


Figure 10 – Model validation for test T1

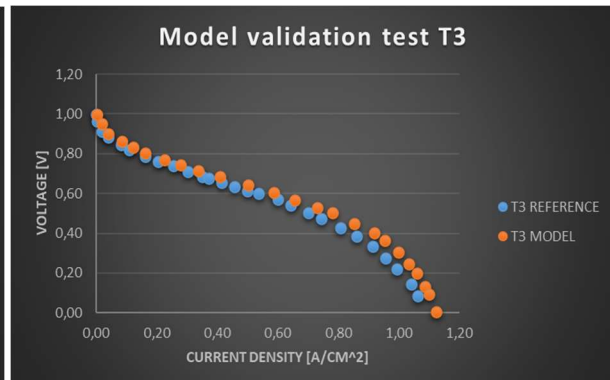


Figure 11 -Model validation for test T3

The figure above shows how precise the model can be, in fact the rest T1 is perfectly stackable and test T3 is stackable above 0.6 voltage that is the usually minimum working condition. The reason of this little difference for high current density is probably to attribute to a different parameterization of relative humidity values between the COMSOL model and the reference one. The COMSOL model provides a single and unique value of relative humidity at current collectors, instead the reference model provides the possibility to insert different values for each collector (both cathode and anode). To complete a correct simulation, when, as in test number 3, the humidity values at the collectors were different between cathode and anode, they were averaged to assess the goodness of the model.

The model is really complex and it provides a huge number of data and graphs. Some of them will be explain in the following sections but there are other graphs the model provides and I want to present them to the reader to make him understand that level of depth reaches the model. As an example, the graphs below are referred to the test number T1.

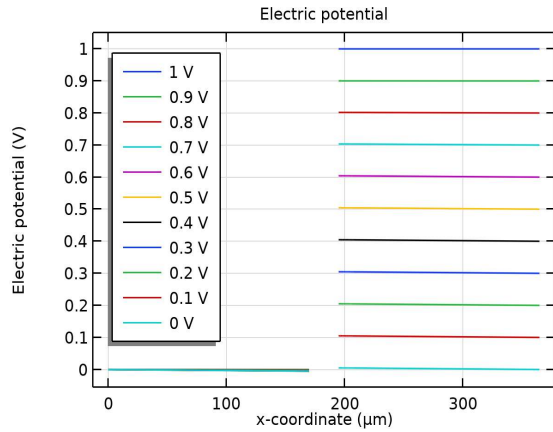


Figure 12- Electric potential

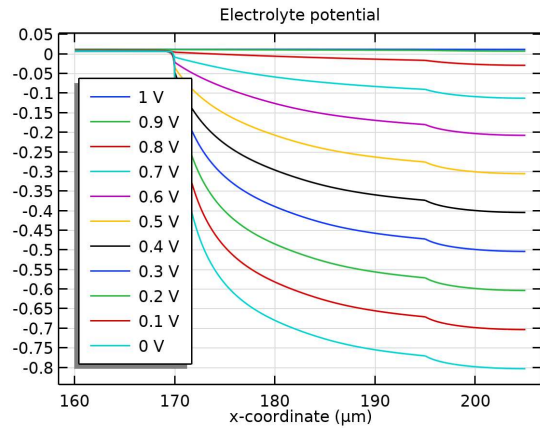


Figure 13- Electrolyte potential

In figure 12 is presented how the electric potential develops inside the gas diffusion layer and constant values can be observed for each cell voltage. On the other hand, in figure 13 it is shown the voltage profile from the point of view of the electrolyte: here it is noted that the typical distribution of the cell is not linear as it was in the electrode but goes towards variations inside the ionomer decreasing from the anode to the cathode. The electrolyte phase potential exhibits an important curvature in figure 13 due to a great variation of proton conductivity. It happens because there is a huge decline of λ toward the anode.[19]

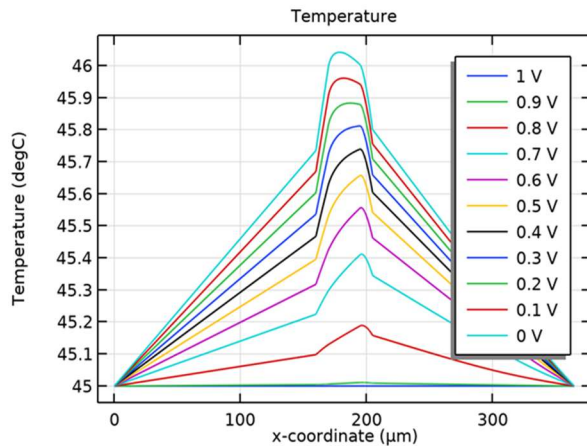


Figure 14- Temperature distribution

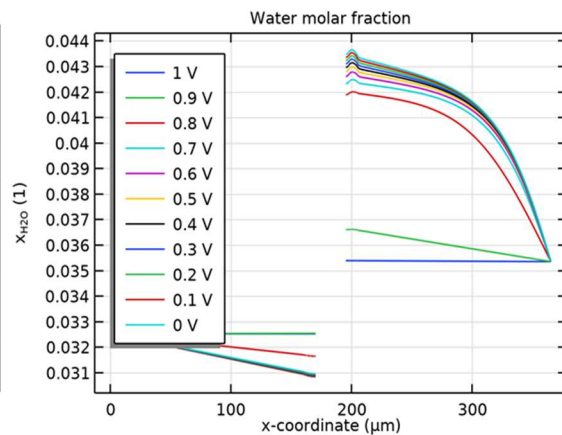


Figure 15 – Water molar fraction

Figure 14 represents the temperature profile of the cell and the reason why there is a pick shortly before the geometric centre of the cell, with the most pronounced increase located between 160 and 170 μm, exactly in the position of the cathode catalyst. This is due to the function of the catalyst that it is able to speed up the chemical reaction: in fact, the oxidation of hydrogen is a dissociation reaction that releases energy in form of heat resulting in an increase of temperature.

Continuing the presentation of the graphs returned by the model and not used later in the discussion, in the figures 15, 16 and 17 other fundamental parameters for cell analysis are shown. These parameters are the molar fractions of the main chemical molecules participating in the cell reactions (water, hydrogen and oxygen respectively). The maximum of water molar fraction is around 200 μm and this is due the combined presence of the catalyst layer and the

high temperature. In fact, the amount of water vapour presents into the cell is a function of saturation pressure which in turn depends on temperature. In addition, the cathode catalyst layer is the end of the reaction cycle leading to the production of water, which justifies this trend.

In figure 16 is presented the rate of hydrogen consumption in the anode side before that hydrogen could reach the anode catalyst layer and it could be oxidised.

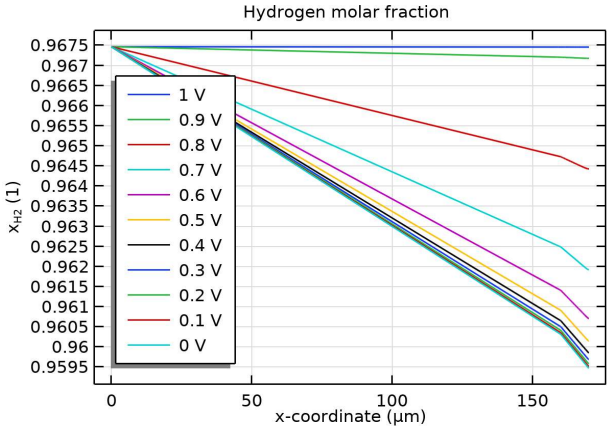


Figure 16 – Hydrogen molar fraction

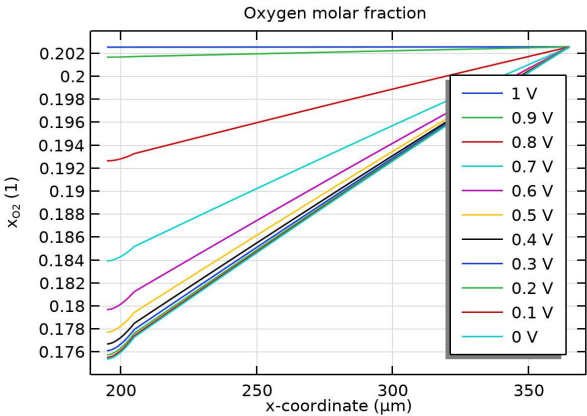


Figure 17 – Oxygen molar fraction

The last graphs that are given as a model output but which will not be mentioned in the thesis are the graphs related to the heat transfer, the hydrogen flow and the oxygen flow inside the cell.

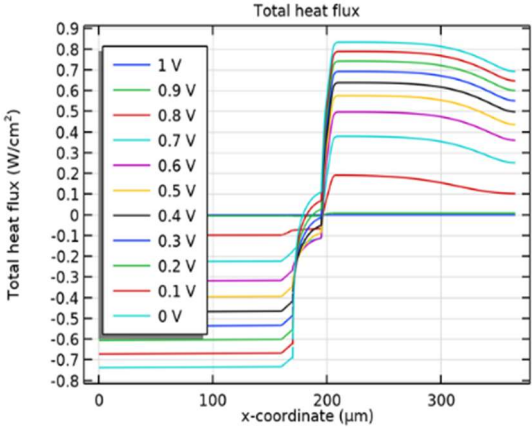


Figure 18 – Total heat flux

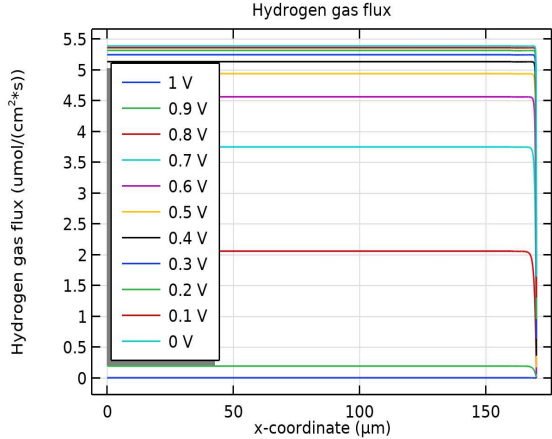


Figure 19 – Hydrogen gas flux

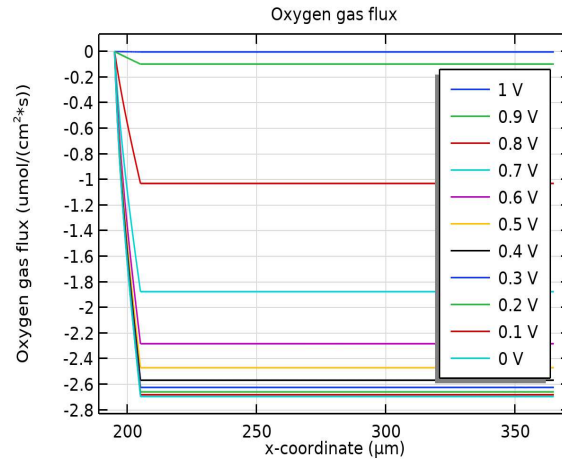


Figure 20 - Oxygen gas flux

Figure 18 shows the heat flow inside the cell. As always in thermodynamics, the heat flow is taken as positive when energy leaves the system, while the sign is negative when the system requires energy from outside.

In figure 18 there is an inversion of the heat flux inside the graph. In fact, the function seems almost perfectly an odd function, but it is not so analytically because, however small, there are heat losses in the transport. It is not surprising if we think the energy is not created but transformed, and this is the essence of what happens inside the cell: the energy contained in the hydrogen is transformed through an electrolytic process into an electric current, with losses in efficiency.

The remaining graphs (figure 19 and figure 20) instead show the flows of hydrogen and oxygen along the longitudinal development of the cell.

Last element to be examined is the drop observed in the hydrogen flow: the drop can be seen from the beginning of the layer corresponding to the catalyst present in the anode, this is due to the fact that the hydrogen activated by the catalyst reacts releasing the electric charge.

I will not show for each step simulation all these graphs because they are not so different one to another. I will focus on polarization curves and other crucial graphs I will present.

4. Experimental procedure

In this section I will show a typical experimental procedure carried out in my case in the laboratory of Politecnico of Turin. First, I will show the ink preparation procedure in the chapter 4.1. In the second section (4.2), I will explain how the experimental curves are evaluated at different temperature and moisture conditions.

4.1 Experimental preparation procedures

As it has been explained in the introduction (1.6), there are different possible catalyst deposition methods with different results in terms of catalyst surface active area. Finding the best deposition method and performing it at the best physical conditions (temperature, humidity) can enhance cell performances. In my experimental activities I worked only with sonification method.

In laboratory I had followed the sonification procedure to understand deeply how this procedure influence performances. With the aim of sonicate the ink, the instrument in figure 21 is used:



Figure 21 - Ink sonification

To successfully complete this procedure, a thermostatic bath is done with ice to prevent the ink from becoming blackened as the procedure significantly increases its temperature as it is described according to several papers: a huge amount of temperature during ink mixing will directly negatively influence cell performance. At the opposite, experimental results show that temperature control of mixing tank improves the process, in fact high temperature can damage the inks and the mixing process is more efficient when temperature is kept close to ambient one.

My first test in the laboratory was focused to simulate how paper results are performed. For the first test an acid solution for the experimental procedure was performed: a solution with Perchloric acid, 0.1 M is prepared into distilled water. The amount of solution required was 75 ml, solution in which the catalytic ink was inserted internally and the procedure for its production is described as follows. The standard procedure for the catalyst inks production was carried out using typically around 5 mg of active catalyst substance, which was subsequently dispersed in the ratio isopropanol: with the following ratio 36.7: 1.65 (water): 1(Nafion, typically). [23]

In the experimental procedure, sonification of ink is done at 55% of maximum frequency of the instrument for 20 minutes with the ink inside the water previously cooled at 4 °C and this temperature is taken constant inserting some ice inside the external water tank. Then, after 20 minutes under sonication, a volume of 3 μ l of inks solution (Pt/C and Pt3Co typically) was extracted and deposited the glassy carbon electrode (GC) to be dried by the "spin coating" technique at 300 rpm. When the ink is dry (figure 22) it looks very homogeneous and regular in surface. Otherwise, when the dry procedure doesn't work it seem irregular with some white points in the middle.



Figure 22 - Ink deposition

At this point of experimental procedure there are some tests to perform. The first one is the cycle polarization curve (figure 23) that is made by saturating the acid solution with nitrogen in static condition. This test shows if our procedure has been completely successfully or not and the path that have to follow is the one reported below (figure 23) and an example of my experimental test for this section is reported in figure 24.

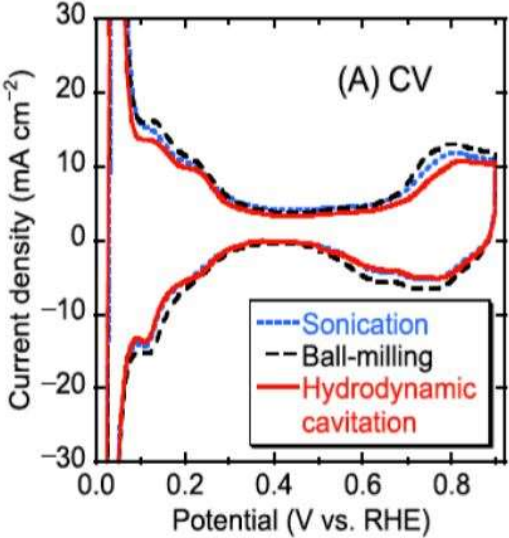


Figure 23 – Typically cycling polarization curve [19]

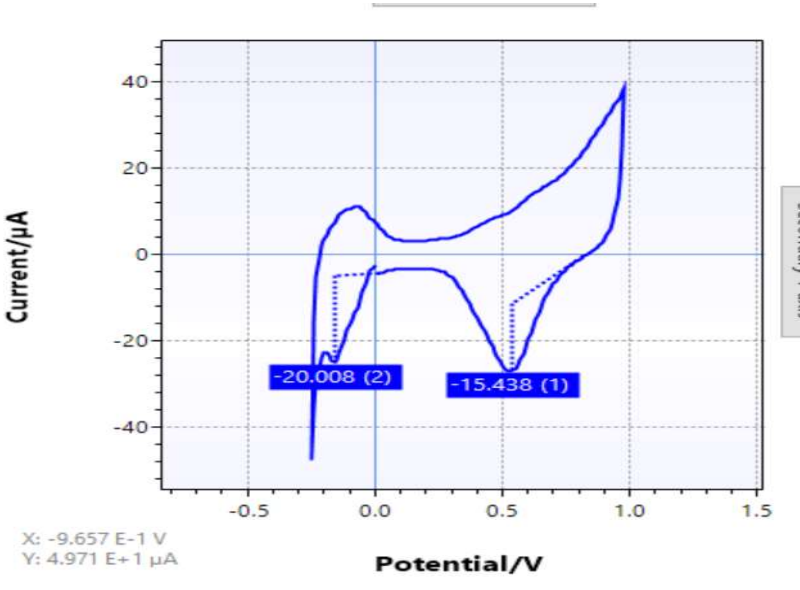


Figure 24 - Cycling polarization curve in Lab

The following procedure will make to verify the voltage and current profile of the deposited material, this procedure is made in the same solution used before but saturated by air.

In this condition, the disk can rotate at 900 rpm and two different procedures are followed:

- Backward;
- Forward.

The Backward procedure consists in setting the initial voltage at the maximum voltage available in the experiment and the final voltage sets to the reference voltage of electrode (set at -0.204 V). (Figure 25)

The forward procedure consists into the reverse setting of the backward (Figure 26) with the maximum voltage available as initial voltage and the final one setting at -0.204 V.

All these processes described before and those that will be described later are made at ambient condition, in September and October of 2021.

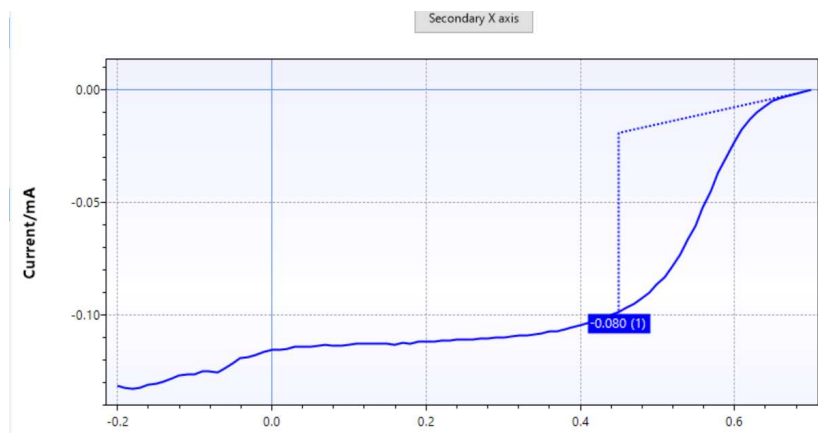


Figure 25 – Backward test

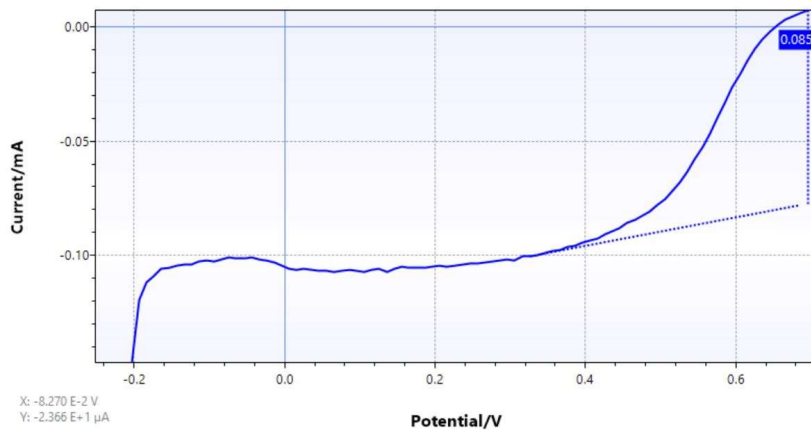


Figure 26 – Forward test

4.2. Catalyst performance evaluation at different temperature conditions

The main purpose of my experimental procedure was to understand how temperature conditions interact with fuel cell's performance. I said before the experimental procedure didn't involve cell analysis but his behaviour was simulated thanks to the COMSOL model described before in section 3. Therefore, I could evaluate just theoretically cell behaviour thanks to the physical equations described before. On the other hand, the evaluation of real behaviour of membrane was possible because of the experimental procedure conducted directly on it.

For what concern the temperature experimental technique, the goal was to create a thermostatic water condition where performing the measure submerged our acid solution and the ink deposited inside. This procedure should have been done for different level of temperature, verifying different cell behaviour for each condition.

Practically, it was less easy than it looks because the rotating ink instrument is very small so the main issues was practically: the tank was too big for the principal instrument and that's why the first procedure didn't work. The second possible procedure was related to heating plate on which I was going to fix the acid solution and the rotating disk. Although it was less bulky compared to previous solutions, it didn't work for the same reason. The last possibility was to use an enveloping jacket that could allow the external circulation of a thermo-heated fluid and that was able to heat the acid solution present inside it (as it is shown in figure 27).



Figure 27 – The system used to perform thermostatic measurement

At this point of experimental procure some insurmountable issues were born:

- the circulation pump was too weak to guarantee a correct circulation and the thermostatic conditions were not satisfied.
- other people in the laboratory needed the thermostatic tank for a continuous period of one month.
- I have not the right laboratory experience to obtain perfectly comparable results for ink procedure.

For all these reasons, in accordance with my thesis supervisor, we decide to focus my attention on the analysis of literature results and the elaboration of them on COMSOL model that can provide correct comparisons starting from solid data with the aim to reduce the approximations.

5. COMSOL Cell comparison

To evaluate the cell behaviour, I search on literature some available data for two of the main companies producer of fuel cell membrane and their description with ionomers differences analysis are reported in chapter 5.1. In the following chapter (5.2) are reported the simulations carried out for 5 different technologies of membranes and the comparative studies among them for different temperature and moisture conditions

5.1. Typology of membrane evaluated

The experimental procedure has the function to provide the best possible polarization data at specific and controlled conditions. In fuel cell application, at the time of writing, Nafion is the reference product for the PEMFCs market and is produced by Dupont, which holds the intellectual property rights.

The Nafion basic chain is define as long side chain and it is basically chemically composed by repeating groups CF_2 among which a group is linked to a branch composed of molecules that give life to this definition (LSC), branching shown in its entirety in the figure 28. [24][25]

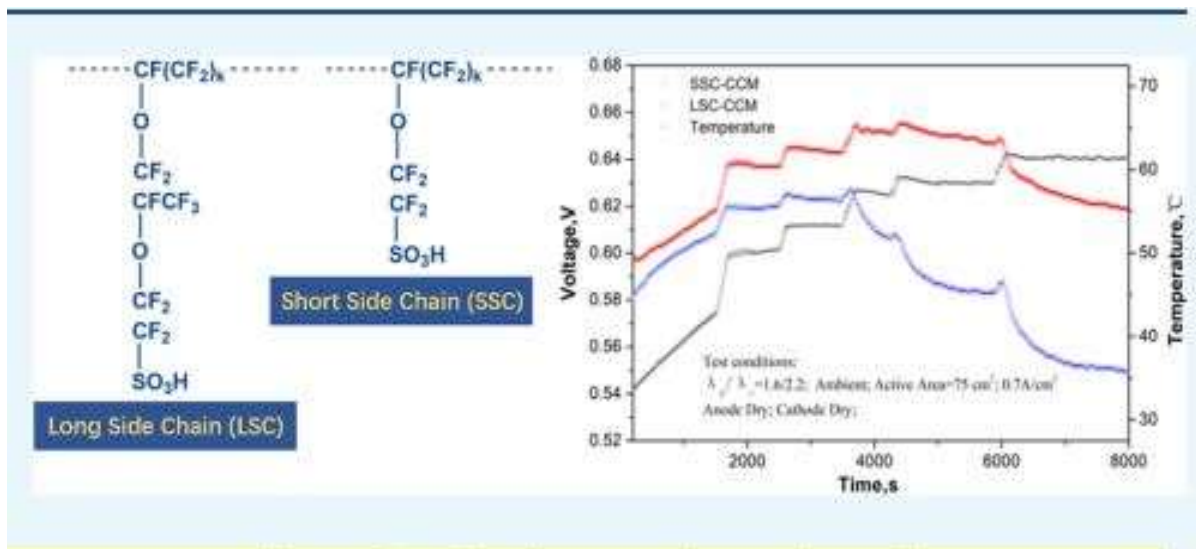


Figure 28 -LSC and SSC [24]

The most important competitor is surely Aquivion membrane produced by SOLVAY: this technology is very promising because it declares to perform better than NAFION at low moisture conditions. This is due to the Aquivion higher water uptake. This aspect in the economy of scale is very promising one because it allows to reduce the size of humidification system or remove it completely. The Aquivion membrane is defined as short side chain and as it is shown in figure 28, the base chain is the same one but it reproduces a different kind of ramification chain, shorter than the competitors one.

In order to perform the simulation of cell behaviour, I decide to evaluate five different membrane typologies: a Nafion standard membrane and four other Solvay Aquivion membranes, that I will list in this chapter. [25][27]

To evaluate their performances, I searched the best data available in literature. For Nafion there are a huge amount of data available for different typology of membranes but sometimes data are also very different one to another. Instead for Aquivion the literature is not so wide and it's difficult to find data to verify their accuracy.

There are several differences between them and not only for the chemical point of view. First, there are some crucial physical parameters that each experimental procedure has to verify, as for example, proton conductivity in function of temperature or relative humidity (RH) and diffusivity in different RH conditions. After these crucial parameters, thickness and the equivalent weight are other fundamental aspects to consider in order to perform a valid simulation.

The main differences used in the model are reported in the table below (Table 7):

	Thickness [μm]	Equivalent weight [g/cm^3]	Density at $\lambda=11$ [g/cm^3]	Volume fraction of water in ionomer at $\lambda=14$	declared proton conductivity at 80°C RH 100% [S/m^2]	Constant for protonconductivity evaluation [S/m^2]
NAFION 211	51	1100	1,79	0,32	17,6	137
AQUIVION E87	50	980	1,93	0,36	22,8	136
AQUIVION E98-05	50	980	1,93	0,34	16,0	109
AQUIVION E98-09S	90	870	1,93	0,34	16,0	110
AQUIVION experimental evaluation of proton conductivity	50	980	1,93	0,34	13,9	94

Table 7 - Membrane characteristics comparison [24] [25] [26] [27] [28] [29] [30] [31] [32] [33] [34] [35] [36] [37] [38] [39] [40] [41] [42]

I modified the model to adapt it to the parameters found in the literature. The first change I made is the change in geometrical properties of membrane with the correct definition of the membrane's thickness. The model does not consider certain mechanical properties to simplify modelling and therefore I changed only the parameters in table 7. All the others geometrical properties are taken constant and they are reported in chapter 3 in the table 5. The second step is to evaluate ionomers properties: the model requires equivalent weight and the density of ionomers to perform the simulation. I found some useful data in the work of Sadeghi and Jankovic where the density is reported in function of λ for each typology of ionomers. [36] Obviously in a mixture ionomer and water, the density of the mixture is in function of their ratio: the main aspect is the ionomer density is related to λ factor and this is due to the relationship between the elements that are part of it.

That's why the density can change with the amount of water as is reported in figure below (figure 29).

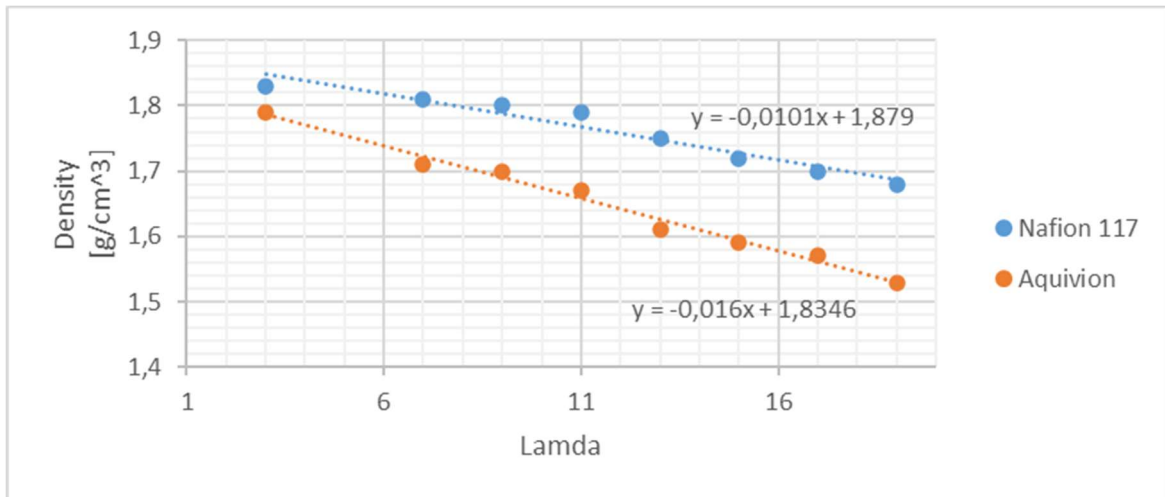


Figure 29 – Ionomers' density variation in function of lambda. [36]

The data available in the graphs (figure 29) are taken from the work of Malek and Sadeghi [35] and I present them in the same plot in order to make a better understanding comparison. It's clear that also density should change with the water content variation but usually we take a constant value to simplify the processing.

Membrane diffusivity can give different results too and it can depend on the water content λ , as is presented for example in figure 30 where it is reported how it changes for Aquivion membrane.

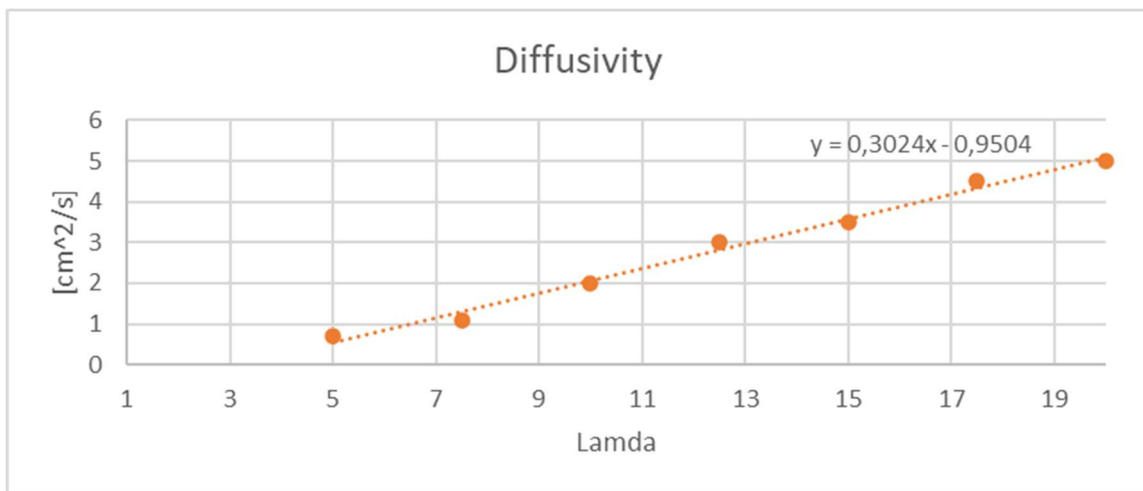


Figure 30 – Ionomers' diffusivity parameters in function of Lambda [36]

At the end, the last parameter that influences deeply the cell behaviours is the proton conductivity. For Nafion the literature for this parameter is wide, sometimes it gives also very different values. Instead for Aquivion the literature available is poor to date and this is due firstly because Nafion is much more widespread from a commercial point of view, now it's the reference typology presents on the market. Secondly for the lack of data is the recent improvement made by Solvay to reach the level of Nafion, improvements which are not yet fully available in the literature data.

From a physical point of view, is clear that proton conductivity is directly proportional with the increase of temperature that gives a great help in the proton transport phenomena.

Proton conductivity is one of the most important parameters for increasing performance, nevertheless there are also other parameters that can interfere with performance, such as the adjustment of the water content.

For this reason, another aspect to consider is the water change of state that can give irreversible damages: this regulation is crucial and it requires a correct compromise between cell performances and safety working conditions. Finding the perfect compromise between these two aspects is essential to ensure security condition and to maximize the cell potential.

My attention was mainly concentrated into the research of scientific papers that could not only attest the maximum available values of proton conductivity, but also to verify their solid foundation in literature. For this reason, I looked among a vast number of scientific publications to cross-all the available data and to certainly affirm if they were isolated cases or if there were confirmations.

After these passages I can evaluate in COMSOL model the comparison among the traditional Nafion's membrane and some Aquivion's membranes. To be precise, the membranes involved in my analysis were the following:

- NAFION 212
- AQUIVION E87
- AQUIVION E98-05
- AQUIVION E98-05 with proton conductivity evaluates experimentally
- AQUIVION E98-09S

For AQUIVION E87, E98-05, E98-09S I used the data reported in the technical schedule that I found on Solvay website. [43] [44] [45] In order to have a more accurate validation of the Aquivion membranes, I decided to perform a simulation based on the characteristics declared by the manufacturer for the Aquivion E98-05 but with the proton conductivity data found in the literature.

Firstly, I started my evaluation from NAFION membrane with the change of some of the initial parameters reported in table 5 with parameters reported in table 8. At this point, looking at the literature, I supposed, for each typology of membrane, to verify some crucial working conditions points and underline the difference with worst ones.

I decided to perform two different kinds of simulations:

1. At constant temperature conditions (80°C)
2. At constant relative humidity at current collectors conditions (RH=90%)

With the purpose of performing a correct evaluation of proton conductivity, I adapted some of the equations reported in the 2.1.5 paragraph. The first hypothesis in my mind was to linearize data collect in literature and use them with the evaluated equation. Unfortunately, this strategy presented some convergence trouble and I had to think something different.

At this point my idea was to exploit a coefficient that could be evaluated in a reference condition and keeping the trend dictated by the Arrhenius equation constant, evaluate the performance also in the other points. Obviously, this solution provided lower reliability compared to the previous method but is certainly more effective.

The parameters evaluation for Nafion 211 was less easy than expected because the aim was to find some reference values at the same physical conditions of relative humidity and temperature. The document written by Lufrano and Simari [26] evaluates proton conductivity at high temperature too but not the same of technical schedule of Solvay. For this reason, I took the evaluate parameter at 80°C and RH equal to 90% and the value reported was 15.7 [S/m] but the comparison was at RH 100%. At this point, looking at the work of Texeira and Sà [31], I evaluated how the variation of proton conductivity was influenced by RH.

I took the angular coefficient that I obtained from the linearization of those values and at that point I had to calculate the ordinate at the origin obtained by imposing the proton conductivity value at the experimental conditions (RH=90%).

At the end of this procedure, I obtained the following equation which gave me a final proton conductivity value of 17.59 [$\frac{S}{m}$] at RH=100% and T=80%:

$$\sigma = 0.1893 * RH - 1.373$$

The same procedure was performed for the evaluation of proton conductivity of Aquivion's membrane with experimental values reported from document 8. The evaluation of angular coefficient for the proton conductivity gave the following equations:

$$\sigma = 0.2332 * RH - 9.4653$$

This equation results at the condition of 80 °C and 100% RH a value of proton conductivity equal to 13.9 [$\frac{S}{m}$].

Looking at the literature, Aquivion membranes are more efficient in diffusivity than Nafion [36] and consequently I assume to estimate an increase of 10% in diffusivity performances in the absence of any other precise information. This approximation does not interact as much for typically voltage working condition while it influences more the maximum value of current that is not interesting for what is my treatment.

5.2. Constant Temperature simulation

For this step of simulation, the maximum temperature is set looking at the literature. I must set 80°C as temperature limit in order to create a correct comparison among different typology of membranes, in fact the Aquivion technical schedule was referred to that kind of temperature. At this level, I decide to evaluate at 4 different moisture conditions evaluated at current collectors for all the typology of membrane:

- A. 80°C at 25% RH
- B. 80°C at 50% RH
- C. 80°C at 75% RH
- D. 80°C at 100% RH

For each point of evaluation, I will report polarization curves for the 5 typologies of membrane considered.

5.2.1 80°C and 25%

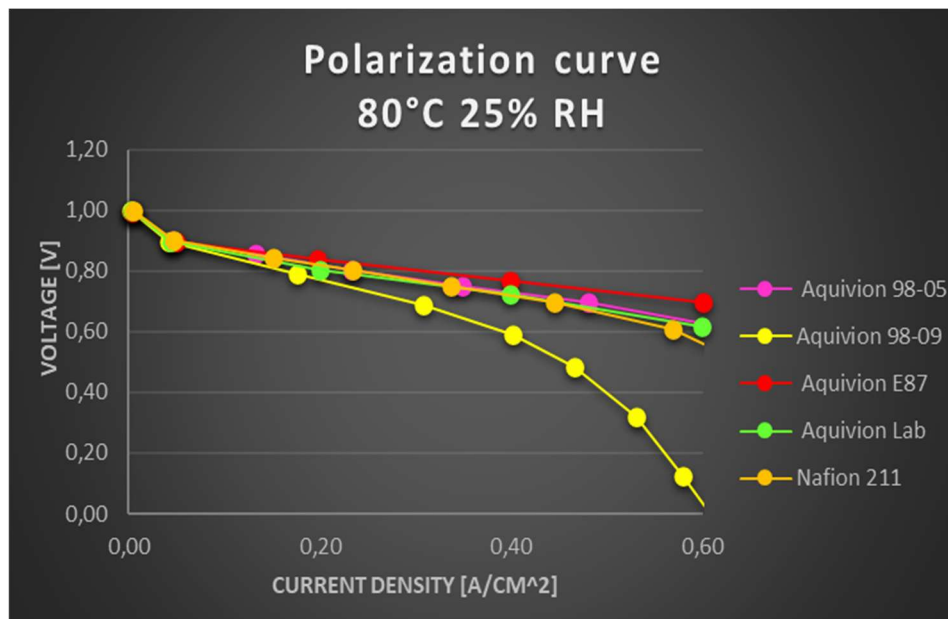


Figure 31.A– Polarization curve at 80°C and 25% RH

The image above (figures 31.A) is related to the five simulations provide for 353 K and relative humidity of 25%. As it will be clear after the following simulations, looking at the temperature-imposed simulations, this set shows the lowest results and this is due to the direct correlation between relative humidity and cell performances. For the same reason the results reported below will provide better working conditions.

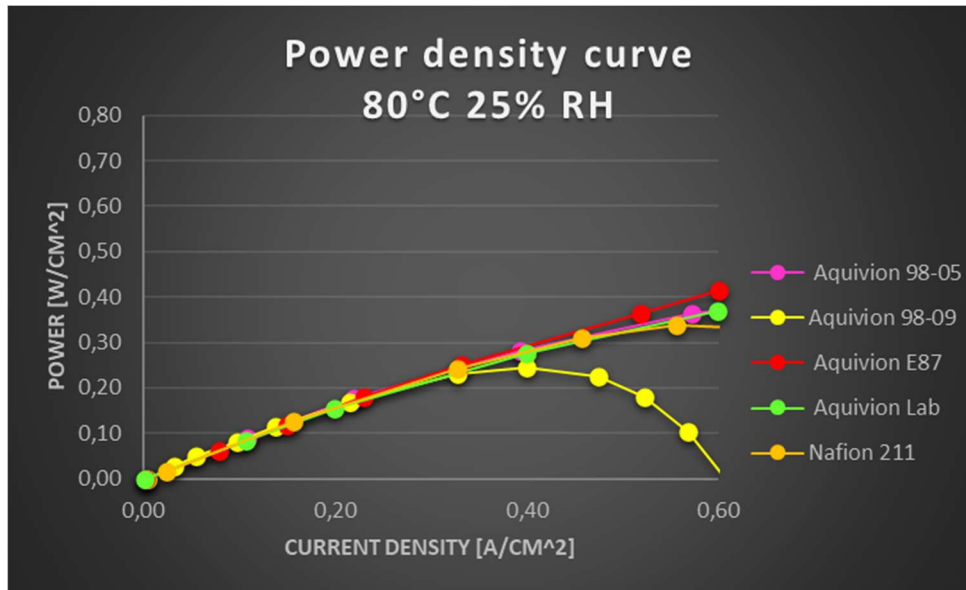


Figure 31.B – Power density curve at 80°C and 25% RH

The figure 31.B is the power curve graph and inside it there are the curves for the membranes considered. This figure is strictly dependent on the previous one since the power curve is obtained from the product of the values of the polarization curve.

For this set of simulation, the Aquivion E-87 membrane shows the best polarization curve and so the best power curved compared to all the other simulations. This performance is due to the best cell parameters as proton conductivity for example.

5.2.2 80°C and 50% RH

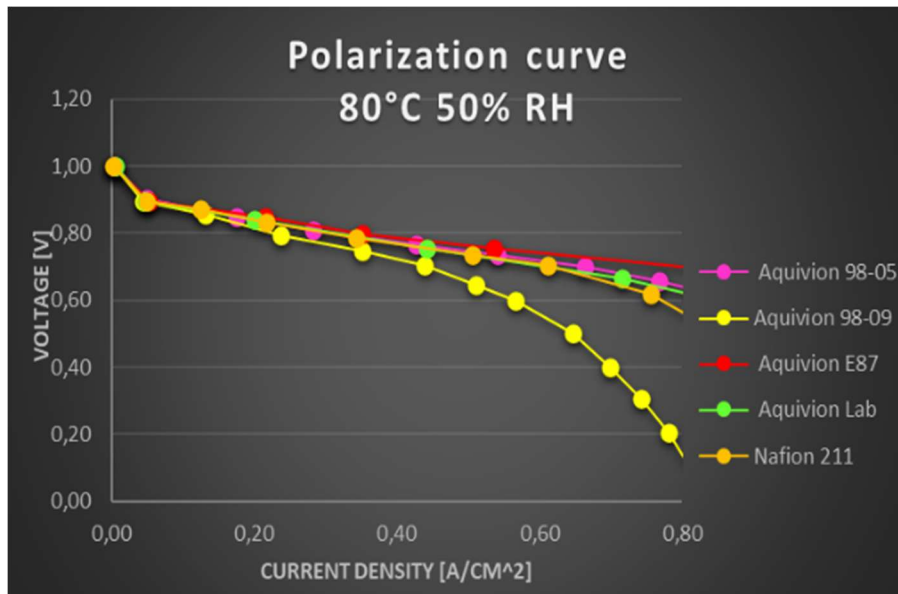


Figure 32.A – Polarization curve at 80°C and 50% RH

The images reported for this set of simulations are related to the five simulations provide for 353K and relative humidity at current collectors of 50% (figure 32.A and 32.B).

In order to do a comparison between this step of simulations and the step before, I evaluate the voltage at $0.5 \frac{A}{cm^2}$ for the Nafion 211 membrane: at the same temperature conditions (80°C), the curve simulated at 50% of relative humidity at current collectors shows 0.732 V while the at 25% of RH shows 0.657 V.

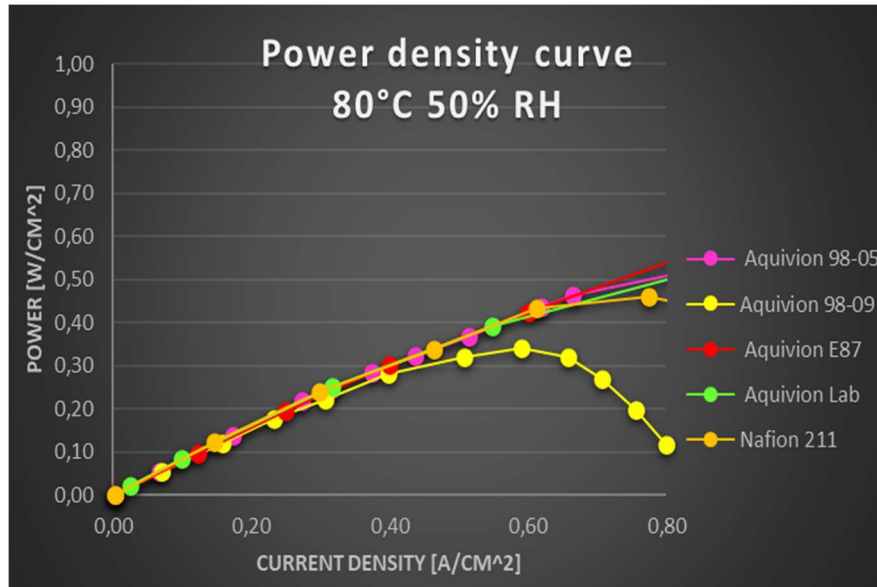


Figure 32.B – Power density curve at 80°C and 50% RH

As it was for the previous working conditions, the best performances are evaluated with the Aquivion E87 membrane, which seems to be really promising compared to the other typologies of membranes showing similar values of power density and current - voltage profile.

Comparing this set of simulations with the previous one there are a significative increase in performances. More specifically, each membrane shows significant improvements over the same type of membrane but at lower relative humidity conditions, this is due to the relative humidity parameter greatly influences the transport phenomena inside the cell, which result in an improvement of the polarization and power curve.

5.2.3 80°C and 75% RH

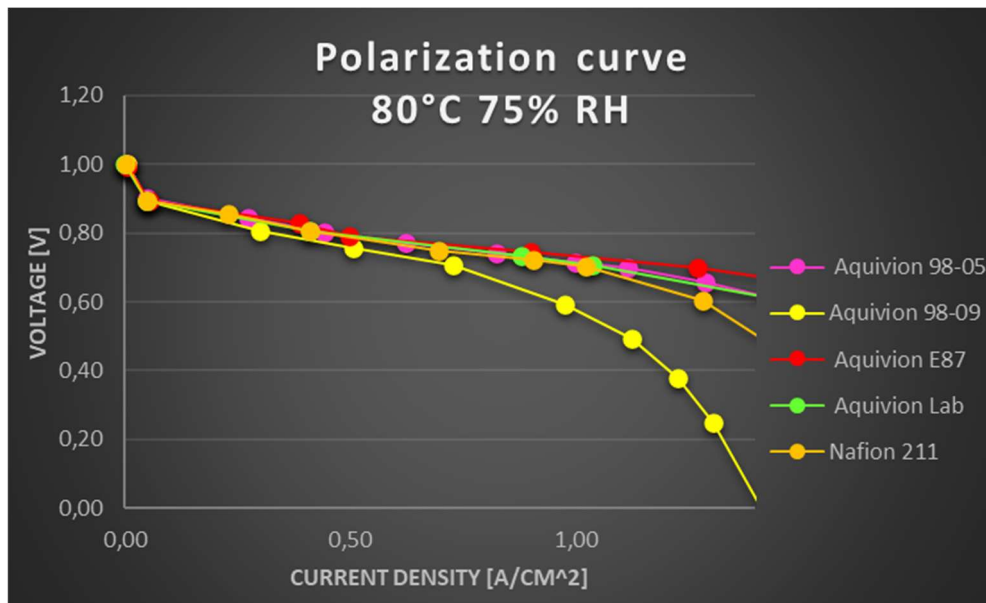


Figure 33.A – Polarization curve at 80°C and 75% RH

Comparing the pairs of graphs 33.A with 32.A and 33.B with 33.B, it is possible to see an increase in relative performance with the same membrane. The increase in performance is present for all membrane types and is most visible in the power curves. This is due to a considerable increase in the moisture content at the current collectors, which reaches a value of 75% in this simulation.

It should also be noted that in this first chapter are considered all simulations at the same temperature level.

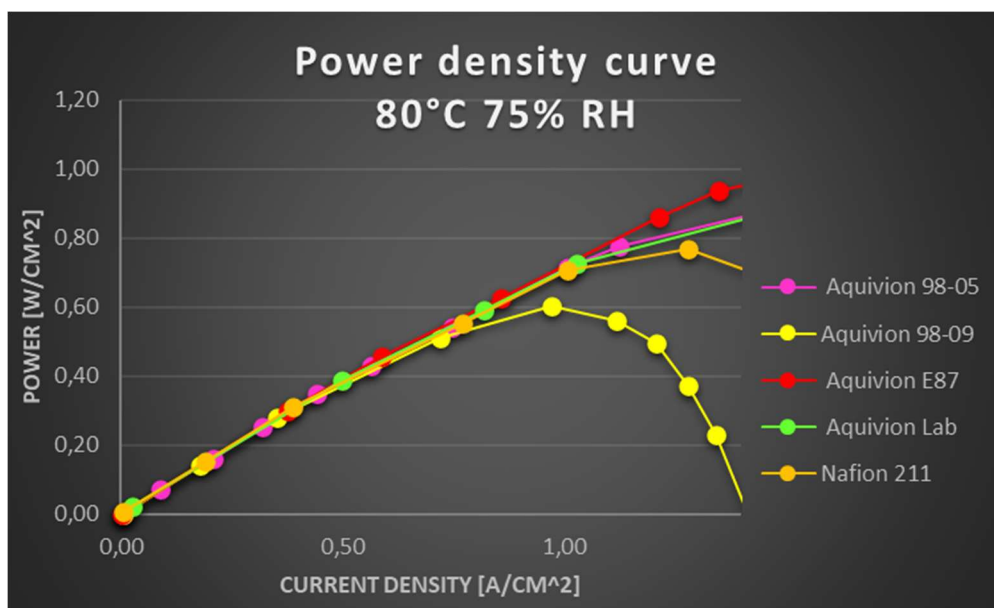


Figure 33.B – Power density curve at 80°C and 75% RH

The following chapter instead will present the maximum cell conditions simulated in this thesis. This is because we are at the maximum conditions evaluable in temperature: not because

the cells do not work at higher temperatures but because 353 K is the temperature considered for the evaluation of cell parameters.

For this step of simulation, I want to provide a comparison between this step and the previous one for Aquivion E98-05 power curves. At 80°C and 0.5 $\frac{A}{cm^2}$ the power value for 75% of RH is 0.398 $\frac{W}{cm^2}$ while for 50% RH condition the simulated power is 0.361 $\frac{W}{cm^2}$

5.2.4 80°C and 100% RH

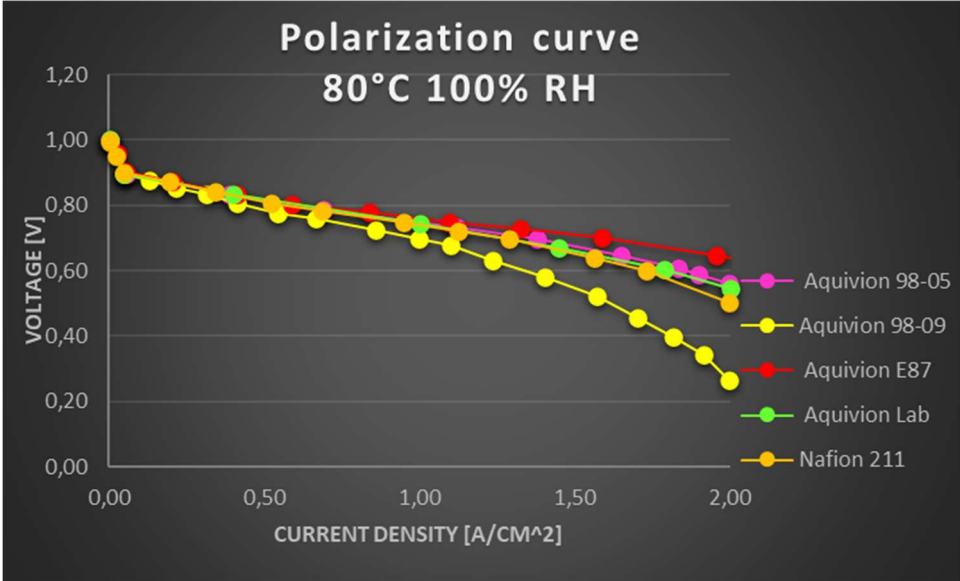


Figure 34.A– Polarization curve at 80°C and 100% RH

The graphs reported in this section (figure 34.A and 34.B) are the best evaluable working conditions for the available input data. In figure 34.A polarization curves are shown for all the membrane typologies, on the other hand the figure 34.B presents the correspondingly power curves.

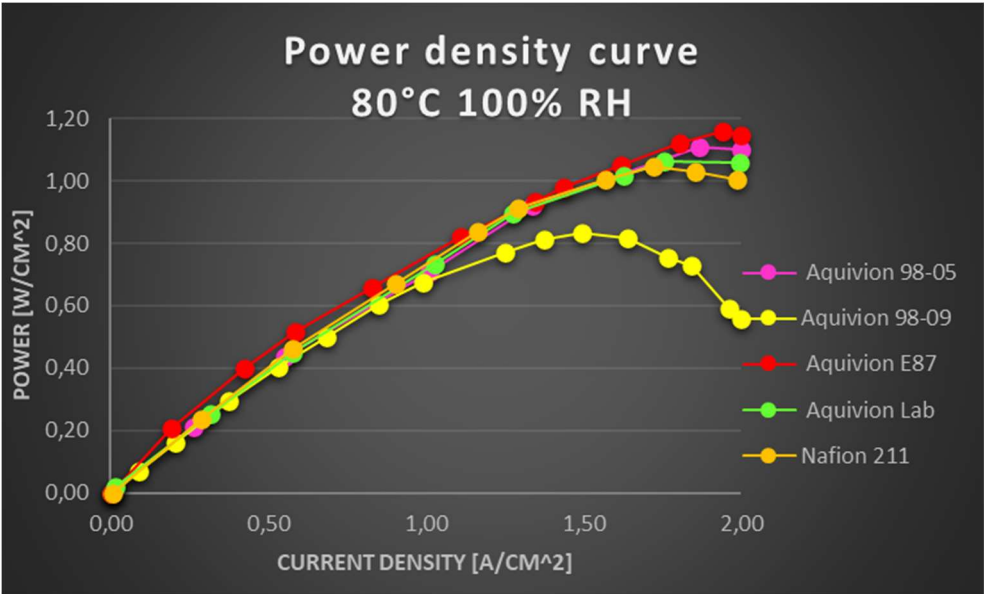


Figure 34.B – Power density curve at 80°C and 100% RH

Being the optimal situation, I decided for this paragraph to report a comparative table to perform an extensive analysis on the simulated performance of the simulated cell, in the same working points considered crucial by the paper considered in chapter 3 (table 8).

	Aquivion E98-09S	Aquivion E98-05 LAB	Nafion N211	Aquivion E98-05	Aquivion E87
U[V] at 0,1 A/cm²	0,888	0,889	0,890	0,891	0,891
U [V] at 0,8 A/cm²	0,739	0,756	0,759	0,769	0,782
Cell power [W/cm²] at 0,8 A/cm²	0,578	0,589	0,592	0,598	0,611
Maximum power [W/cm²]	0,822	1,059	1,040	1,118	1,178
Evaluation conditions at 80°C and RH 100%					

Table 8 - Performance comparison of different membranes

In table 8, there are the comparison of principal simulation data, sorted from left to right for maximum power output at $0.8 \left[\frac{A}{cm^2} \right]$.

Analysing the data in table 8, we see that as the current density is reduced, the curves do not deviate much from each other, giving almost identical values. For increasing values of current density, higher deviations are observed. The same behaviour is shown graphically into the figure 35.

The simulations shows that Nafion's membranes is similar to the traditional Aquivion membranes, except for the E87 typology that presents incredible high results and it opens the way to new and more efficient application of fuel cell. If the data will be confirmed after more precise analysis, Aquivion E-87 could reduce the general cost of cell for the same power output or increase the power output taking the same cost.

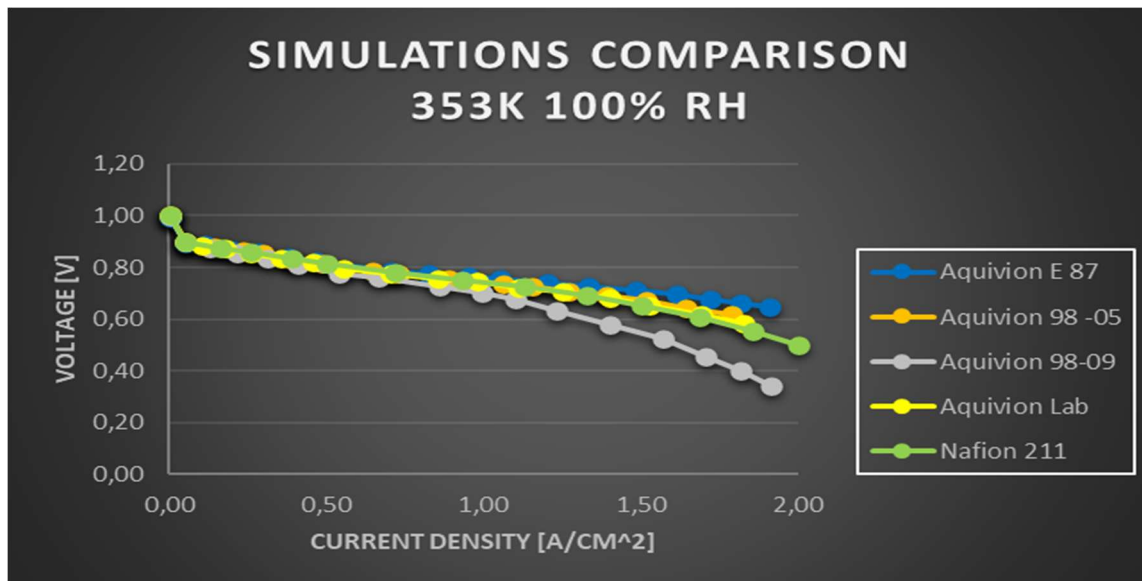


Figure 35 – Simulation comparison at 353 K and 100% RH

In figure 35, I took all the simulations performed at 353 K and 100 % of relative humidity at current collectors to present how they perform compared to the other.

The figure above shows us an overall view that allows us to have a more complete judgment on what are the orders of magnitude of difference between one type of membrane and another. This graph gives the perceptive of the not excessive difference between the various types of membranes and of how much the data of Aquivion E-87 membrane bring the respective simulation to the top of performances.

Concerning Nafion performances, the data in table 8 and the figure 35 show there are not so huge differences at typical working condition. It is crucial to consider that Nafion data are more reliable because there are several feedbacks in the literature. Instead, especially for the values declared from Solvay for Aquivion E-87, not so many feedbacks are available today.

In conclusion, I want to underline the lower performances provided from Aquivion E 98-09. This is an old typology of membrane with high thickness value (90 μm) and not so high value of proton conductivity $16 \frac{\text{S}}{\text{m}}$.

5.3. Constant relative humidity simulation

The last crucial simulation I retain to perform is the variation of temperature at constant moisture condition. For this simulation level, I decide to set relative humidity parameter at 90% as constant value with the following step of temperature.

- A. 90% RH at 30°C
- B. 90% RH at 50°C
- C. 90% RH at 70°C
- D. 90% RH at 80°C

5.3.1 90% RH and 30°C

This is the first set of simulations reported for constant values of relative humidity at current collector. These simulations are planned with the purpose of demonstrate how fundamental the role of temperature is and how it can improve cell performances.

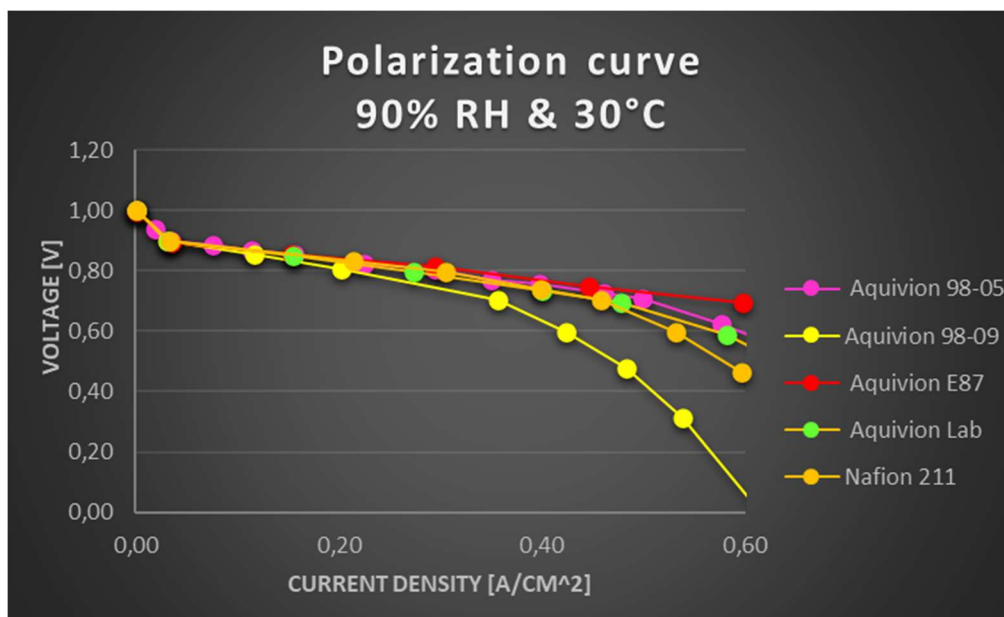


Figure 36.A – Polarization curve at 90% RH and 30°C

After the comparison of these simulations, it will be clear that the increase of temperature induces an increase of performance which manifests itself through a considerable increase of current density and consequently a considerable increase of power.

In figure 36.A is presented the polarization curve for all five membranes considered at 303 K and 90% of relative humidity at current collectors. The same conditions are performed for the power curves available in figure 36.B.

A first consideration that can be made is that membrane performance varies with the applied boundary conditions. However, in this case, the same relative trends of before are shown. Let me explain: the Aquivion E 87 membrane is still the best performing membrane, while the least performing is the Aquivion E98-09S membrane.

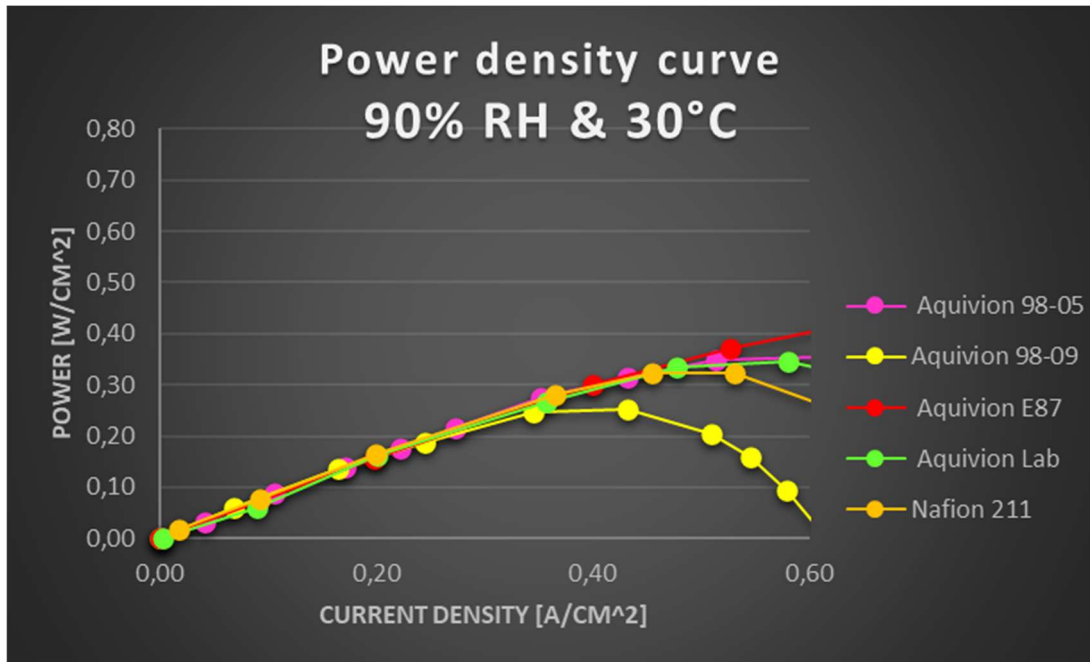


Figure 36.B – Power density curve at 90% RH and 30°C

The power curve shows very low results and this is due to the low temperature conditions. It will be clear that when temperature increase, performances will improve, already from the next simulation.

5.3.2 90% RH and 50°C

This step of simulation is performed at 323 K and 90% of relative humidity at current collectors.

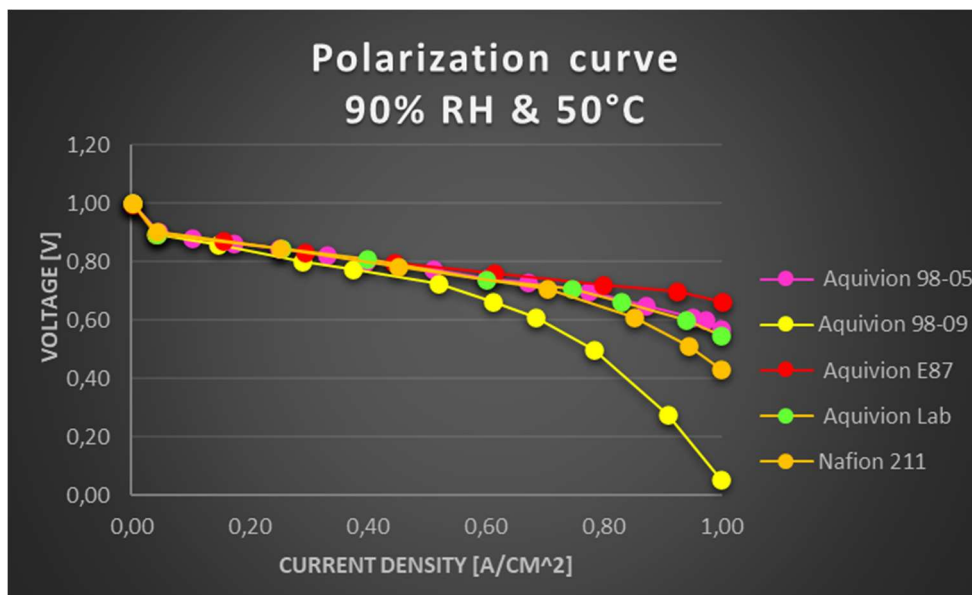


Figure 37.A – Polarization curve at 90% RH and 50°C

Looking at the comparison between figure 37.A and 36.A, it becomes clear that temperatures have a significant effect, not so much on the cell voltage at low currents, but on the currents themselves. The same figures can be seen in order to establishing how temperature determines cell performance: even looking at the comparison between the various power curves, comparing for example figures 36.B and 37.B, I want to emphasise how performance increases with a temperature delta of just 20 degrees Celsius.

To make this comparison more evident, looking at the polarisation curves (figures 36.A and 37.A) we can consider the same current density conditions for the Aquivion E-87 membrane and check how the voltage varies with the temperature. Considering a current density of $0.3 \left[\frac{A}{cm^2} \right]$, the curve at 30°C has a voltage of 0.793 V, while the curve at 50°C has a voltage of 0.829V.

This is analytical verification of how there is a small increase in cell voltages but an improvement that is not comparable to the increase in current densities.

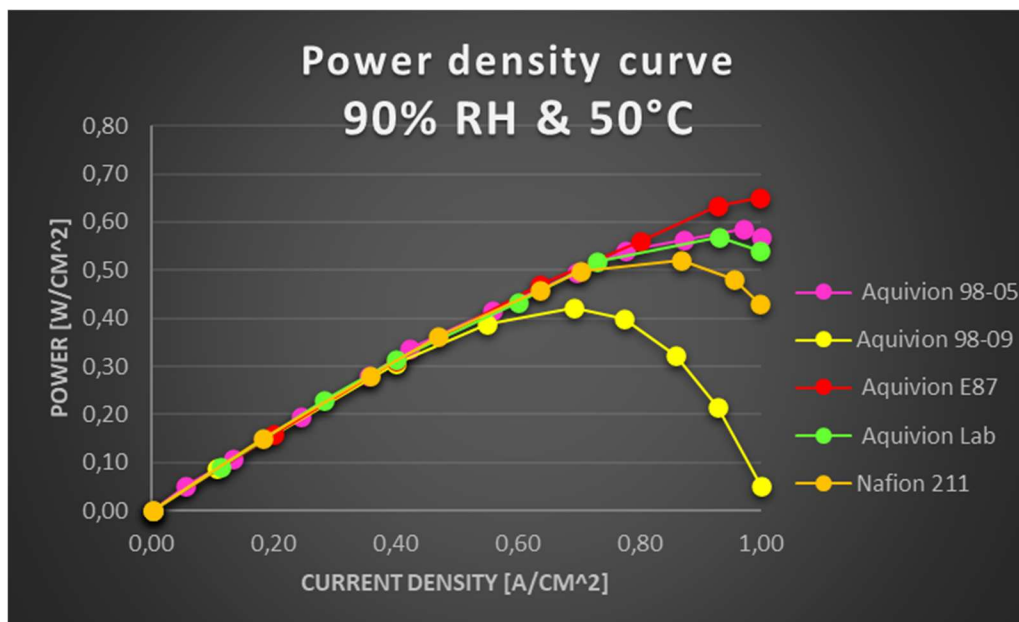


Figure 37.B – Power density curve at 90% RH and 50°C

Likewise for the previous increase of temperature, the following increase will present a huge step forward too. For this step of simulation, I also want to provide a comparison between this step and the previous one for Nafion 211 power curves. At 90% of relative humidity at current collectors and $0.5 \frac{A}{cm^2}$ the power value for 50°C is $0.387 \frac{W}{cm^2}$ while for 30 °C the simulated power is $0.324 \frac{W}{cm^2}$.

5.3.3 90% RH and 70°C

This step of simulation is performed at 343 K and 90% of relative humidity at current collectors. In figures 38.A and 38.B show a further increase in performance which is again due to the increase in temperature of 20 °C.

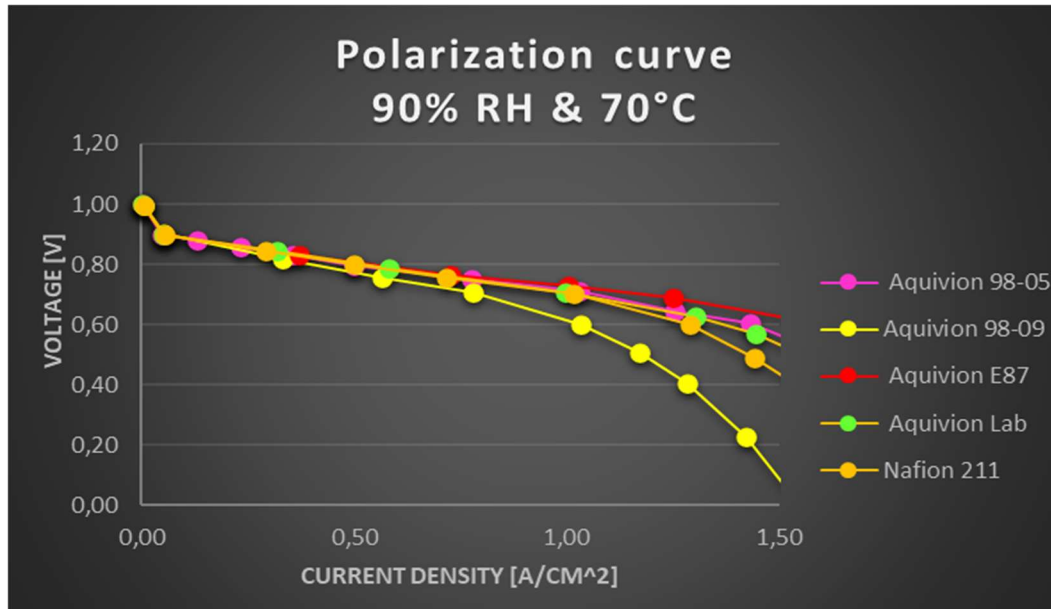


Figure 38.A – Polarization curve at 90% RH and 70°C

As an idea of the performance increase due to the temperature rise of this simulation step, I evaluate the voltage change for Aquivion E-87 at $0.5 \left[\frac{A}{cm^2} \right]$ for figures 37.A and 38.A

The simulated outputs from the model turn out to be a voltage of 0.795 V at 50°C and voltage value of 0.814V at 70 °C, respectively, not such a dramatic difference. This small increase is a recurring feature that has been previously discussed.

But it is not a surprise because the maximum voltage is subjected to the physical limit that cannot be overcome. In fact, the maximum possible physical voltage for a hydrogen/oxygen fuel cell is 1.23V [48].

In the figure below (38.B) there are all the power curves available for the set conditions of this simulations. The discussion for the performances is the same for polarization curves and it is due to the fact that power curves derive from the polarization curve.

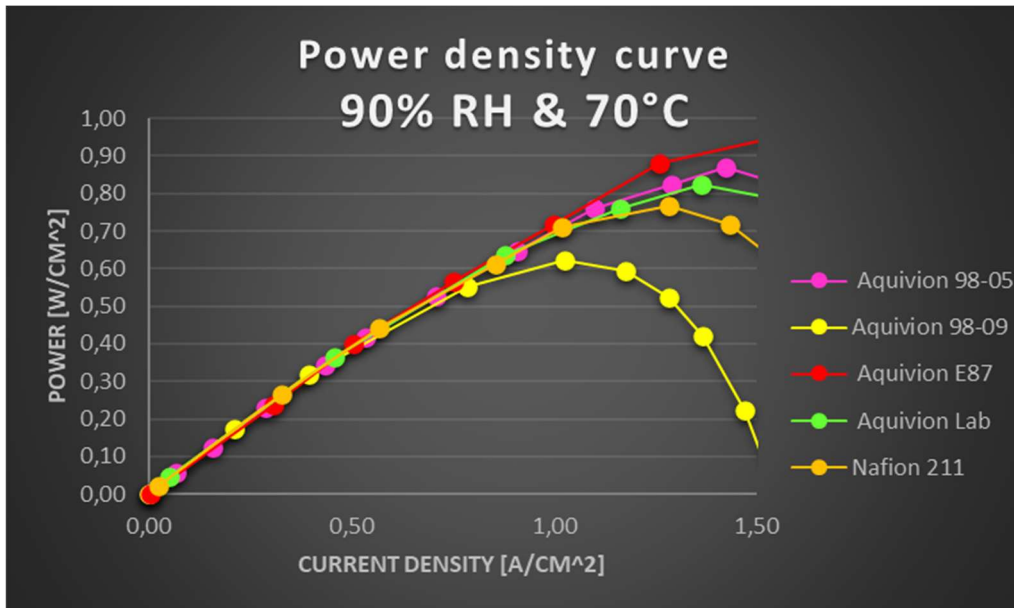


Figure 38.B – Power density curve at 90% RH and 70°C

5.3.4 90% RH and 80°C

This step of simulation is performed at 353 K and 90% of relative humidity at current collectors and it provides the greatest performances of this chapter. These working conditions (figure 39) is not far from the ones presented in figure 34. Here performances are little lower than figure 34 but nearly overlapping and for this reason I will not provide a completely comparison as I did in the chapter before. However, it is useful to emphasize how a 10% increase in relative humidity at the current collector can improve overall performance.

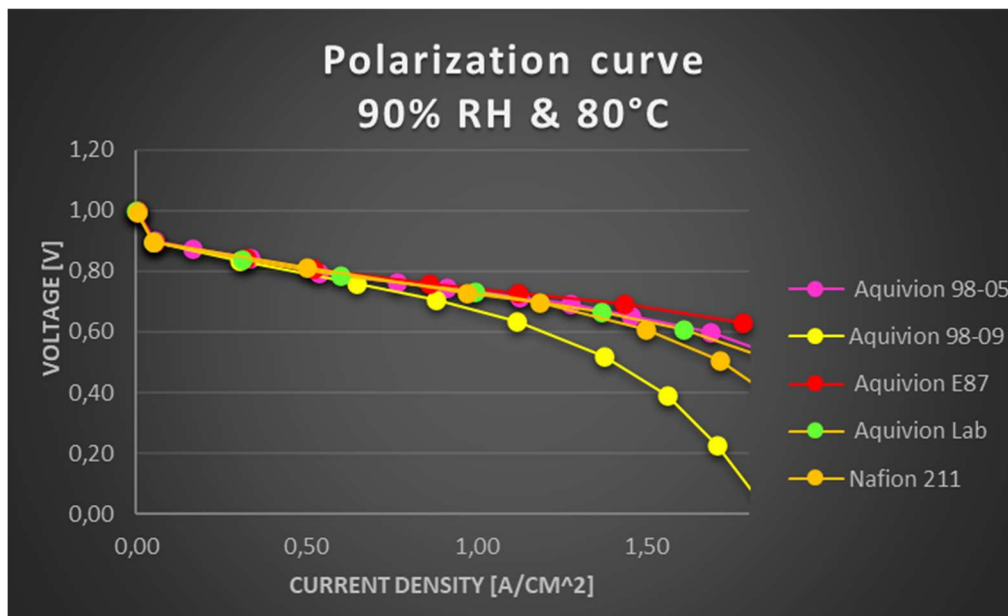


Figure 39.A – Polarization curve at 90% RH and 80°C

In this case, as in all the previous ones, the Aquivion E-87 membrane would seem to be the best performer with higher values, however, it has to be reconfirmed by more in-depth experimental analyses.

In figure 39.B is shown the power density curves: they are similar to the ones available in figure 34.B with slightly lower values. As an example, I report the data of Aquivion E98-05: in figure 39.B the maximum power is $1.013 \left[\frac{W}{cm^2} \right]$ when in the conditions reported in figure 34.B it was $1.118 \left[\frac{W}{cm^2} \right]$.

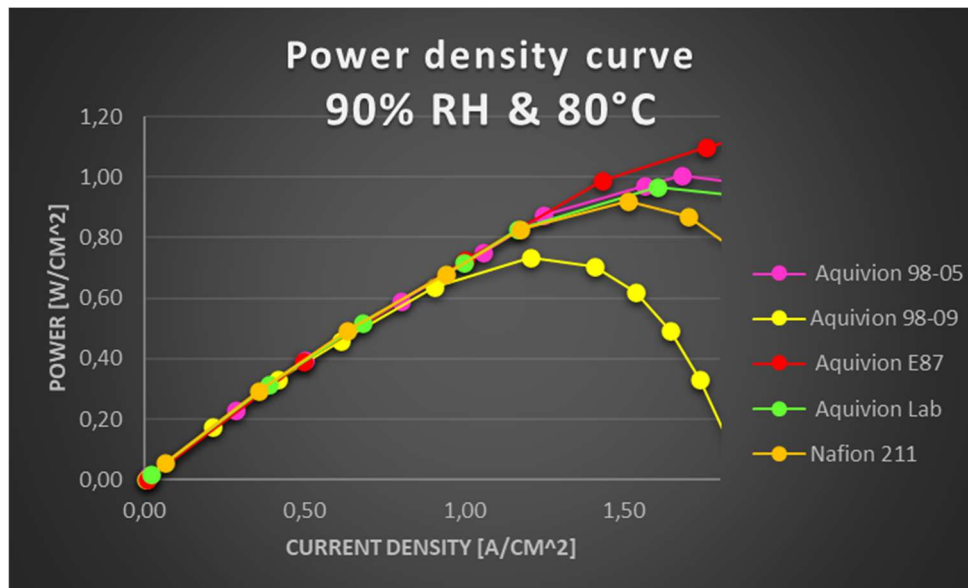


Figure 39.B – Power density curve at 90% RH and 80°C

5.4. Simulations validation through literature comparison

Looking at the simulation output, it is useful, in order to validate the model output, to verify that results are comparable to literature outcomes. To do this, I use the reference data from the work of Cullen and Neyerlin [47] corresponding to the green line in the figure below (figure 40): there are two types of membranes simulated with the parameters described in the previous chapters: Aquivion E87 (red line with filled dots) and Nafion 211 (green line with filled dots).

The first aspect to emphasize is that, graphically speaking, the simulated curves of Aquivion E-87 and Nafion 211 present a trend that optimistically reflects the real one. These membranes are compared with literature data and, after the simulation, it can be seen that the characteristics of Aquivion E-87 declared by Solvay result in a large increase in performances compared to the literature. [47] [24] On the other hand, the Nafion 211 data look very similar to those in literature. To provide a correct comparison, all the following curves are evaluated at 353 K and 100% of relative humidity for each typology of membrane.

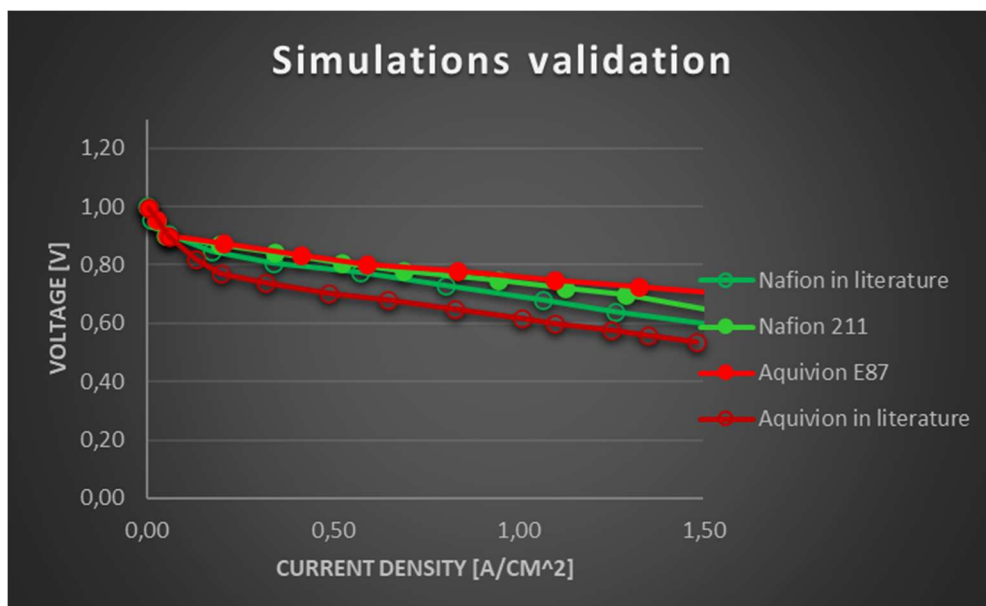


Figure 40 – Simulations validation, polarization curve

For low values of current density, all three curves have more or less the same values. There is a first change of behaviour around $0.2 \frac{A}{cm^2}$ where the Solvay's optimistic data start to be perhaps too optimistic (Aquivion E-87). On the other hand, the Nafion 211 data came from laboratory analysis, so it is correct that they reflect more of the literature data which are also from laboratory analysis. In contrast, Solvay data is the one declared by the manufacturer. For this reason, before certifying that the Aquivion membrane is better than Nafion 211, it will be necessary to carry out other experimental tests that univocally confirm the parameters expressed by Solvay.

The same validation procedure is performed for the power density of cell as it is reported in the following figure (figure 41).

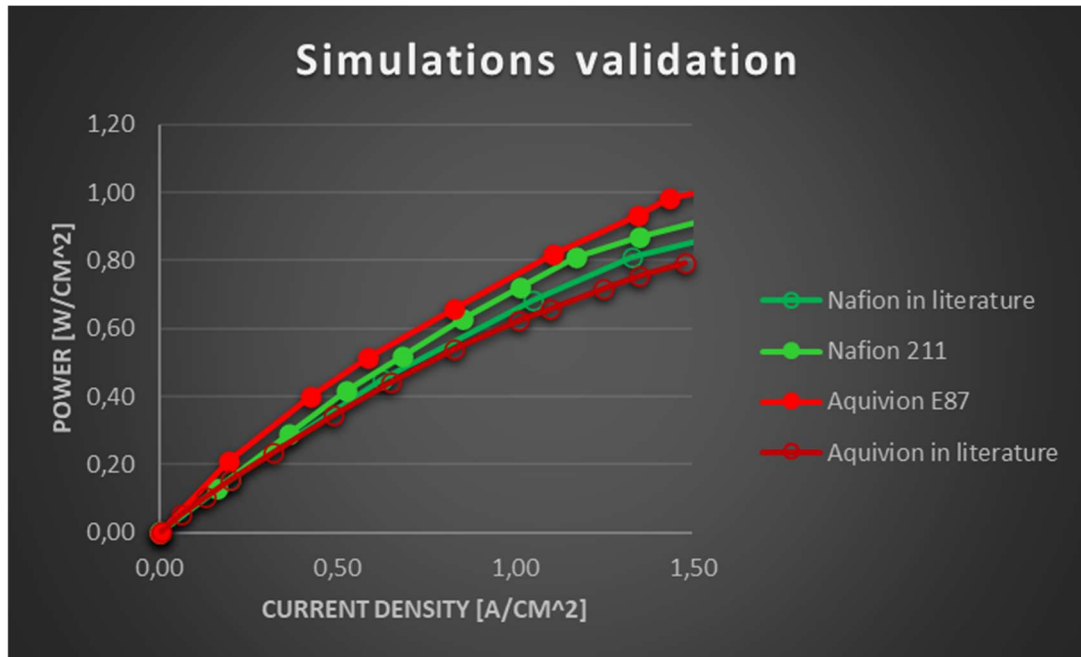


Figure 41 - Simulations validation, power curve

These curves are evaluated for all three typologies of membranes at 353 K and 90% of relative humidity. In this case the literature data for Nafion comes from the paper of R. Jinnouchi and K. Kudo [48] and for Aquivion, it comes from the paper cited before [24].

It is useful to highlight that the power density curve is achieved from the product of current density and voltage so the power curve that would result from graph 40 would be slightly better than the one presented at the same temperature but lower RH (figure 41).

As before, the Aquivion E-87 shows optimistic results, the Nafion 211 reveals similar literature results.

5.5. *Simulation analysis*

As it is shown in table 8, there are some differences from one membrane to another and this underlines the importance of this layer for the overall performance of the whole cell.

As it has been presented before, I want to highlight the big efforts Solvay is making to reach the level of Dupont's products and these simulations show that today the Nafion monopoly is not so sure.

Analysing the data, I decided to evaluate the behaviour of cells in traditional working conditions because under 0.5V some degradation processes start and the cell is not performing as well as it could. For the same reason it is not useful to evaluate performances at maximum current because maximum currents are reached just at low voltage values.

Obviously, these simulations do not provide exact data because the base model and the equation was evaluated looking at the Nafion membranes; however, the correction of the main parameters of the ionomer allows me to affirm that the results are valid with a certain margin of tolerance for the assumptions made during this work.

The cell power evaluated through the simulations returns values that clearly identify the E87 membrane as a more convenient solution and the values reports seem to be coherent with the experimental results provided by the paper cited during this work (simulations validation is available in the previous chapter).

The model is able to simulate different properties and physical phenomena of cell in order to have a better comparison of the performance, I will also evaluate some crucial properties such as:

- Current distribution.
- Oxygen transport.
- Water transport.

Output graphs, which will not be presented below, are available in chapter 3.

5.5.1 Current distribution

The first parameter to evaluate is the current distribution. In this section there are different graphs that show how this parameter varies into the different layers of the cell and how it changes using different kinds of membrane.

As mentioned, the current distribution in a fuel cell varies according to the position within the cell. In fact, there are certain layers in which there is a current transition from the electrodes to the electrolyte. The model presented specifies what is the current density available separately at the electrodes and in the electrolyte. The graphical representation of the above is illustrated in figures 42-43.

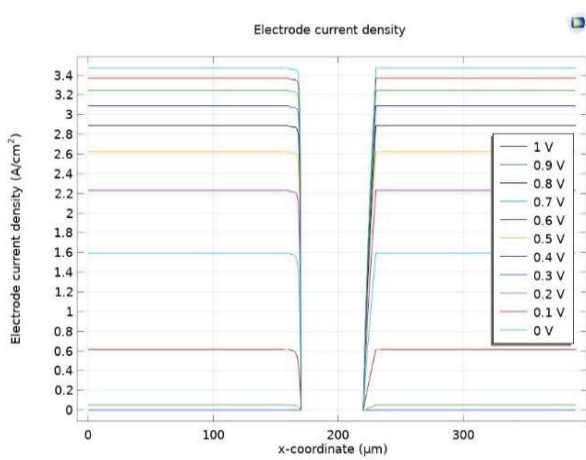


Figure 42 - Electrode current density, E-87

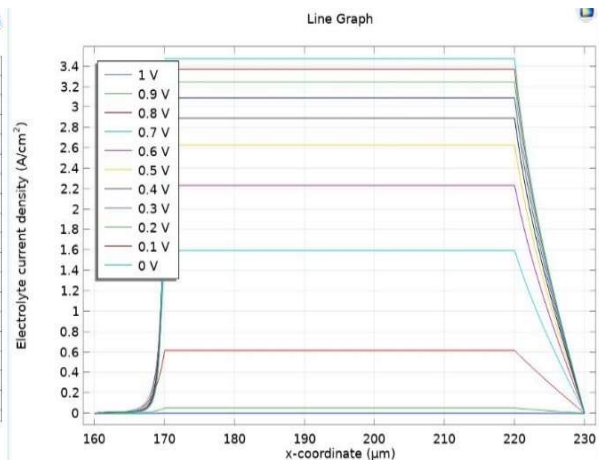


Figure 43 – Electrolyte current density, E-87

Looking at the first figure (figure 42), the electrode current density seems to be constant for each voltage profile respectively and the discontinuity starts around 160 μm . This value has a specific meaning, in fact it is the transition zone between the gas diffusion layer and the anode catalyst layer. This is the reason for the enormous decrease in current density seen in figure 42; on the other hand, it happens the opposite in figure 43 where there is a corresponding exponential increase.[19] This change of layer causes a change in the current distribution evaluation: the current distribution switches from being an electron flux into the gas diffusion layer to a protonic flux into the membrane. The continuity equation tells us that the current varies with the variation of the potential and it explains the trend of these graphs.

$$j_e = -\sigma_e * \nabla\Phi_e$$

$$j_p = -\sigma_p * \nabla\Phi_p$$

To see what is happening more closely, in the figures below I have zoomed on the above figures in the areas of interest. It is interesting to see how there isn't a net passage between one layer and the other, but it seems that they could be mesh one to another in the catalyst layer.

It's crucial to underline that all these figures are reported for 353 K and 100% of relative humidity at current collectors conditions.

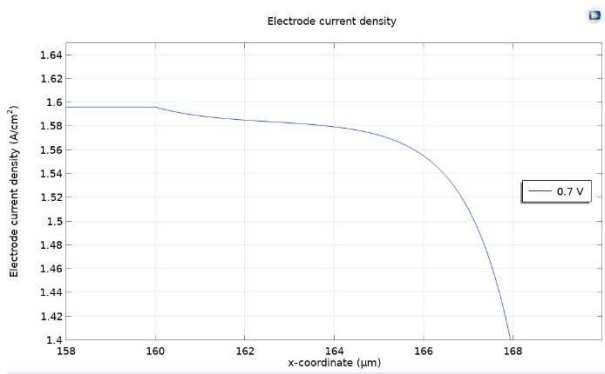


Figure 44 - Electrode current density zooms of the cathode catalyst layer, E-87

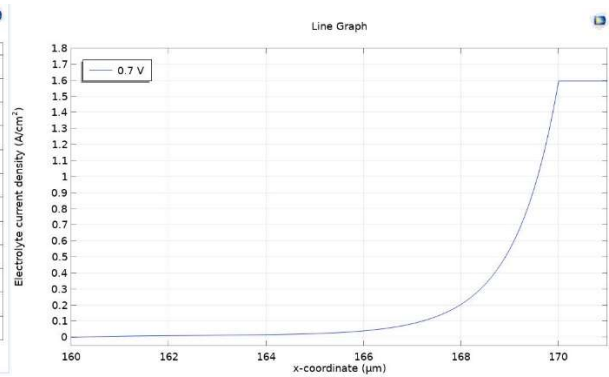


Figure 45 - Electrolyte current density zooms of the cathode catalyst layer, E-87

The physical layers distribution displays that the catalyst layer starts at 160 μm and it ends at 170 μm . In this zone, to better clarify, I concentrate on analysing the curves with an applied voltage of 0.7 V, looking more closely at the transition zone between the layers.

Looking at this specific case, entering in the anode catalyst layer there is a large and steep decrease in current parameters, but this decrease can be modelled in two different trends, as it is shown in figure 44:

- Soft decrease between 160 and 165 μm
- Steep decrease between 165 and 170 μm

This behavioural diversity is due to the proximity of the layer that influences it more. If the catalyst layer is closer to the gas diffusion layer, then the current distribution will be concentrated into the electrode. Vice versa if we are beyond the middle of the catalyst layer, then the predominant influence will be the electrolyte one. Therefore, the current distribution will be concentrated in that layer, as shown in figure 45, where there is an abrupt and exponential increase of the electrolyte current density in correspondence of 165 μm .

The same happens on the other side of electrolyte layer for cathode catalyst layer with specular modality. I want to underline that these trends are function of boundary conditions applied.

I want to compare the same zoomed figures for Nafion 211 to understand if the change of membrane influences or not the current distribution and, if it does, how.

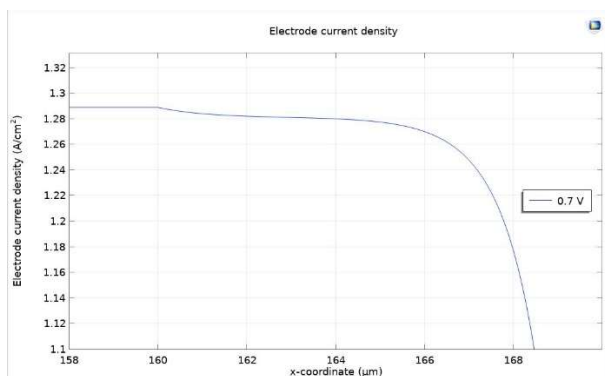


Figure 46 - Electrode current density zooms of the cathode catalyst layer, Nafion 211

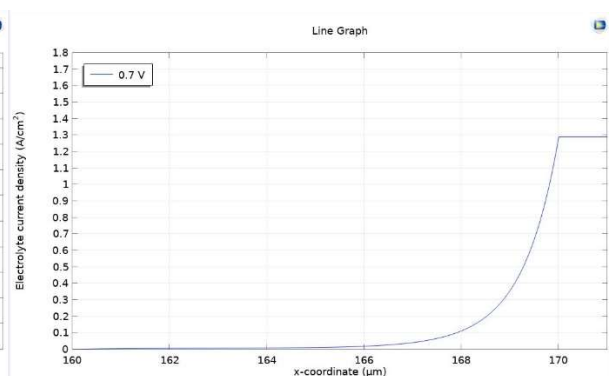


Figure 47 - Electrolyte current density zooms of the cathode catalyst layer Nafion 211

Thanks to figures 46 and 47 that are related to the Nafion 211 membrane, it is possible to perform a correct comparative analysis with the same graphs for the Aquivion E 87 (figures 44-45). For each membrane, I considered the same boundary conditions, such as temperature, humidity and voltage.

Looking at the proposed comparison, the first consideration is related to the analytical value of electrode current density ($1.59 \frac{A}{cm^2}$ for the E-87 compared to $1.29 \frac{A}{cm^2}$ for Nafion 211). The second consideration is that the path of curve is pretty much the same and this is due to the same geometrical conditions and the same typology catalyst layer considered.

Beyond numerical differences, the shape of curves suggests that figure 46 has lightly smoothed discontinuity at the beginning of the catalyst layer compared to figure 44.

To provide literature comparison, I searched for a 3D example of current distributions that could explain better what the real current distribution behaviour is.

The 3D reported below was evaluate by T. Falagüerra, P. Muñoz, G. Correa [49], and it shows a typical PEMFC.

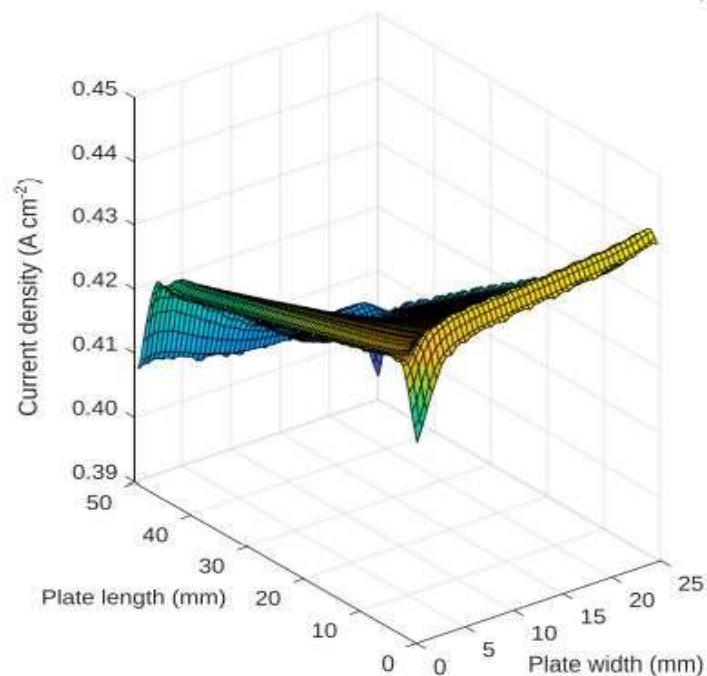


Figure 48 - 3D current density distribution example [49]

In this example, the current density variation is observable from its distribution in the active area width and this is useful because it allows us to consider how the current, and all other cell parameters too, are a function of the chemical reactions, which take place within the cell. Figure 48 shows there are nonlinear distributions into the catalyst layer width, but the comparison of this figure with the ones proposed from our model takes meaning only if we consider the 2D model, so the plate length in figure 48. Comparing this figure with figure 42, there is a corresponding decrease of electrode current density into the catalyst layer. In figure 42 is presented the whole electrode current density, the part of interest for the comparison is the catalyst layer between 160 and 170 μm . Figure 48 shows the same two different behaviours described on the previous page.

5.5.2 Oxygen transport

Some of the key factors for the optimisation of the cell's performance are the study of oxygen transport and the study of phenomena that can affect it. An effective oxygen transport is a fundamental aspect to be studied because the reduction of oxygen allows the closure of the reaction cycle. Ineffective oxygen transport slows down the closing of the cycle, worsening the performance of the cell. In fact, this reaction is a necessary step in the production of water molecules from the oxidised hydrogen at the anode, reactions that are crucial because they enable the electricity production. [51]

The figure 49 present the typical scheme of a fuel cell. This figure helps me to emphasise that the use of oxygen is directly proportional to the amount of hydrogen reacted.

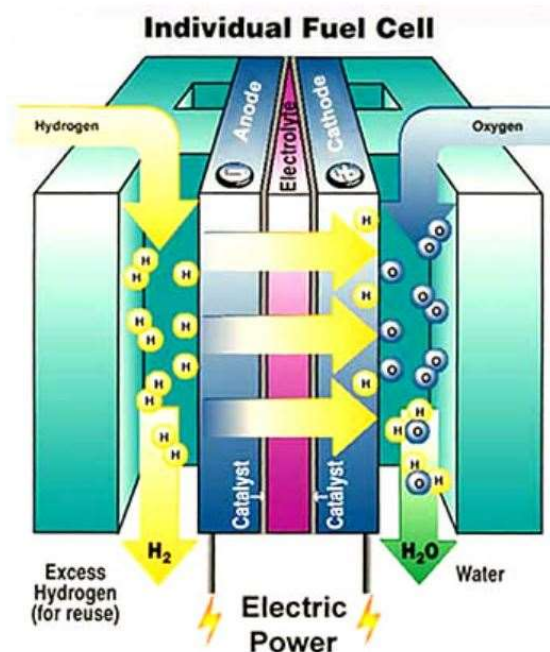


Figure 49 - Typical fuel cell model [53]

To introduce the discussion of obstructive oxygen transport phenomena, we can briefly divide the types of resistance present into two:

- Fickian component resistance.
- Non-Fickian resistance.

Fickian resistances are referred to diffusion processes that can be seen as an obstruction for their pore diameters. The non-Fickian resistances include a great number of phenomena that can directly influence the cell performance, one of them is surely the amount of platinum dispersity in the cell. This process increases in specific weight when counting losses at high current density values, as has been shown in studies conducted by Sun and Yu [51].

Looking closer at the phenomena of oxygen resistance, this is one of the most critical optimisations of the cell. There are a great number of aspects that could be analysed in detail. Thought, I will try to analyse the main ones.

Firstly, the amount of platinum in the catalyst is one of the phenomena that directly influences the oxygen transport: it has been demonstrated that a decrease in platinum content induces an increase in oxygen transport resistance.[48] The results of Jinnouchi and Kudo in the same paper suggest that the main bottleneck for oxygen transport is the oxygen permeation into the catalyst layer.

The influence of how Pt/C particles and ionomer can interact with the oxygen transport phenomena is one of the most analysed phenomena in this field. The oxygen flows into pores of catalyst layer and the way in which this agglomerate is composed influences directly the oxygen transport properties.[52] Pores are another crucial aspect to consider in transport phenomena in general. Looking at the oxygen transport, the change of pore diameters has a huge impact into the gas transport properties and in diffusion mechanisms too.

To present the complexity of oxygen transport, the work of Liang et al. [52] lists the main scenarios that are possible for oxygen, scenarios which directly affect transport phenomena:

- O_2 dissolution from gas pore into the water.
- The O_2 diffusion into the water.
- The O_2 dissolution from water to ionomer.
- O_2 adsorption into the ionomer.
- O_2 adsorption into the Pt surface.[52]

The same model provides a classification of different oxygen transport's resistances by layers. Before introducing this classification of resistance, it is necessary to comment on the image below (figure 50) to show the layers taken into account by the paper.

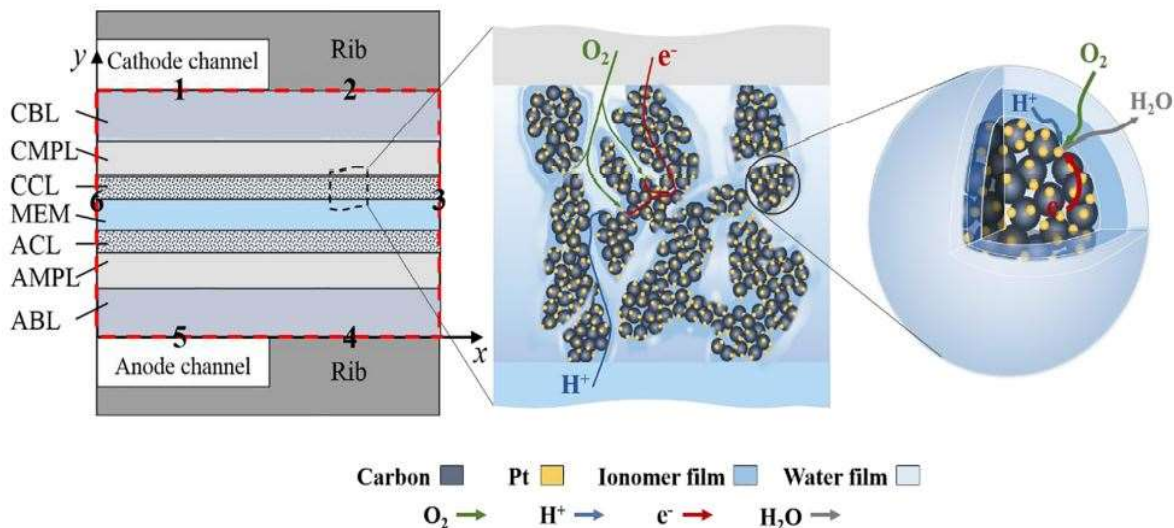


Figure 50 – Central part of the cell and Pt/C and ionomer agglomerate [52]

In figure 50, among the cathode channel and the membrane, there are the CBL, which is the cathode backing layer, the CMPL, which is the cathode microporous layer, and the CCL, which is the cathode catalyst layer.

This schematization is useful to introduce the resistance presented by the model. It provides four different typologies of resistances depending on the layer the oxygen is going through.

The first resistance term is referred to the CBL with the following equation:

$$R_{CBL} = \frac{l_{CBL}}{D_{O_2,CBL}^{eff} * S_{CBL}^{1.5}}$$

Where:

- D is the diffusive term [m^2/s];
- l is the thickness [m];
- s is the liquid saturation [-]. [52]

The second resistance term is referred to the CMPL with the equation below [52]:

$$R_{CMPL} = \frac{l_{CMPL}}{D_{O_2,CMPL}^{eff} * S_{CMPL}^{1.5}}$$

In this case the parameters are the same of the previous equation but they are related to the cathode microporous layer.

The third term represents the catalyst layer's resistances, which are divided in two categories. The first one is the bulk transport resistance with the equation below.[52]

$$R_{Bulk} = \frac{l_{CCL}}{D_{O_2,CCL}^{eff} * S_{CCL}^{1.5}}$$

The other term is local oxygen transport resistance represented with a complex equation different from the previous ones.

$$r_{loc} = \frac{\delta_w * C_{O_2,g}}{D_{O_2,w} * C_l} + H_n \left(\frac{1}{k_n} + \frac{\delta_n}{D_{O_2,n}} + \frac{1}{k_{Pt}} \right)$$

Where:

- δ_w is the thickness of water film [m];
- D_{O_2} is the oxygen diffusive term for water (w) or ionomer (n) [m^2/s];
- k is the adsorption apparent rate constant for ionomer (n) and platinum surface (Pt) [m/s];
- C is the concentration of oxygen ($C_{O_2,g}$) and liquid phase (C_l) [mol/m^3]. [52]

This kind of division is useful to understand if there are changes in some parameters and where these changes can affect the oxygen transport.

An example of how reducing the platinum content affects the catalyst layer is presented in the figure below (figure 51). It shows how this can affect and where oxygen transport finds the greatest resistance.

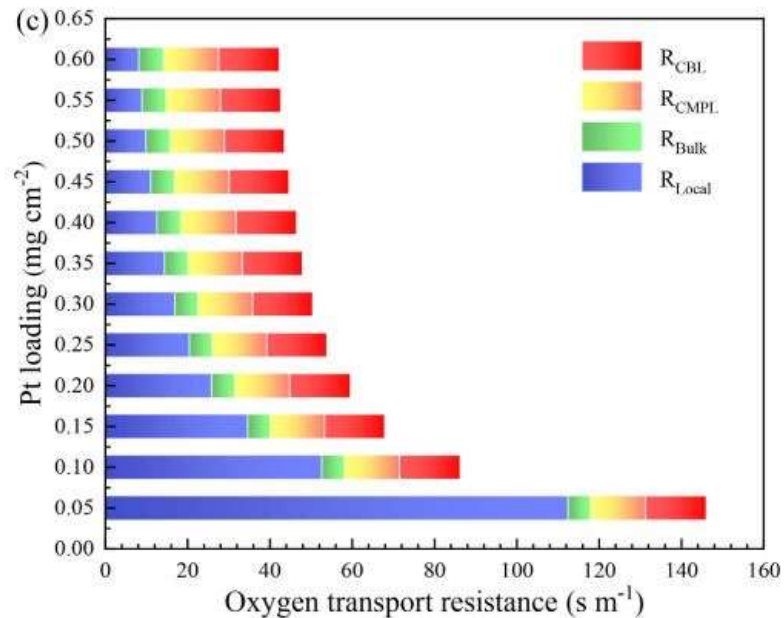


Figure 51 - Oxygen transport resistance in function of Pt loading [52]

Figure 51 is crucial to understand what kind of resistances most affect the oxygen transport. It indicates that the reduction of platinum loading impacts mainly the local resistances into the catalyst layer, which is due to the fact that “the oxygen effective diffusion route in ionomer film becomes longer” as it is explained into the work of Liang et al. [52]. On the other hand, the bulk resistance slightly decreases because of the reduction of the platinum amount.

As it happened for all physical phenomena in the cell, oxygen transport efficiency has a direct impact on other cell parameters, so modelling it is essential to understand how it affects current density. In fact, an excessive obstruction in oxygen transport causes a reduction in the recombination of charge and the water formation processes.[51] In order to do that, in our model, there is a section dedicated to checking how oxygen transport takes place within the cell. The graphs relating to this section are helpful to check how oxygen transport affects cell performances as the input parameters change.

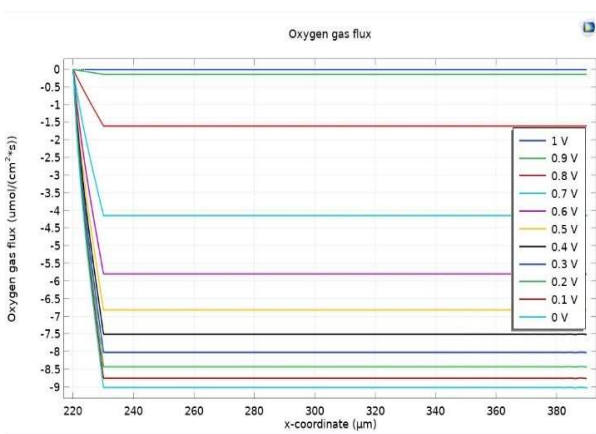


Figure 52 – Oxygen gas flux, E-87

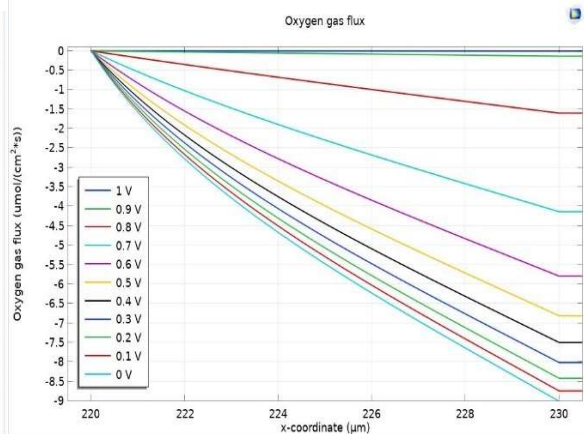


Figure 53 - Catalyst layer oxygen flux, E-87

Figures above (52 - 53) refer to the Aquivion E-87, which has 10 μm of catalyst layer for the cathode placed between 230 and 240 μm. Figure 52 shows the oxygen transport from the cathode catalyst layer to the cathode gas diffusion layer. In figure 53, however, I wanted to highlight only the portion of the cell relating to the cathode catalyst layer: in this section, recombination reactions are activated and oxygen reacts to produce water.

Negative values may seem at first sight a contradiction but it is not if we consider that the inserted oxygen has to react with hydrogen ions and for this reason the negative flux is intended as a decrease of oxygen at cathode.

The model provides a simulation of how oxygen transport takes place in the catalyst layer. The figures above show how cell voltages affect transport phenomena. Oxygen transport has slopes that are a function of the voltage of interest and most of the curves at different voltages appear to be describable as approximately linear.

In order to make an effective comparison, the graphs corresponding to the previous simulations are also presented for Nafion 211 membrane. I would like to remind that the boundary conditions are the same as those used for the current distribution, that are 353 K and relative humidity at the current collectors of 100%.

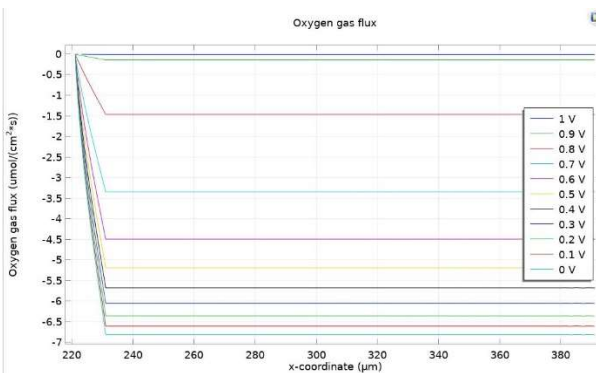


Figure 54 – Oxygen gas flux, Nafion 211

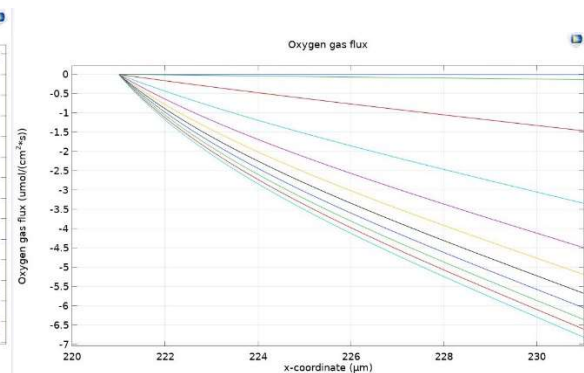


Figure 55 - Catalyst layer oxygen flux, Nafion 211

From a graphical point of view, figures 54 and 55 show similar curves to those of Aquivion E-87 with inequalities for the amounts of oxygen transported. These differences can be attributed to the different capacity of the membrane to transport ions and hence the lower need for oxygen to react. The oxygen flux is modelled using the Fick's diffusion theory so the flow

is seen as oxygen used in the reaction and for this reason is negative. The flux of oxygen starts from position 220 μm because it is the cathode catalyst layer beginning: this is the point at which the oxygen reduction reaction begins. Figures 53 and 55 appear to have the same behaviour. Although, after careful analysis, it can be seen that there is different behaviour at the edges of the catalytic layer, due to the different characteristics of the membrane, since the Aquivion membrane is 1 μm larger than that of Nafion.

The last aspect I want to take into account is the decreasing part of the curve: for Nafion 211 it seems to be less vertical than the Aquivion E-87 ones. The reason is the higher amount of oxygen transported through the E-87 membrane than through Nafion 211, with the same properties of catalytic layers.

5.5.3 Water transport

At this point in the work, it is clear to the reader that the study of each physical phenomenon within the cell is not independent from the analysis of the other cell's phenomena, because these phenomena are interconnected and require an overall study. Keeping this in mind, the analysis of water transport management is another important aspect to consider and it requires a huge optimization process to improve cell performances. For PEMFCs, the correct balance of water management influences the output parameters of the cell: too much water can saturate the cell, obstructing the pores for gas transport, but at the same time an excessive decrease in water content will cause dehydration of the membrane, limiting ohmic and proton conductivity.[54][55]

The analysis of gas-liquid flows within flow channels is a complex subject that requires an overview of various physical characteristics such as the importance of heat transport, how fluid mechanics interact within the system and how this affects mass transport, in addition to the action of electrochemical phenomena in the cell.

In the following lines, I will try to give an overview of the main physical phenomena at work, keeping in mind that the discussion is complex and would require very detailed analyses for each phenomenon I will mention. To avoid weighing down the discussion, I will only consider steady state phenomena, not considering start-up or shutdown conditions.

To discuss water transport, it is necessary to consider that simulation models frequently assume ideal current and temperature distributions, but this is not always the case in ordinary cell dynamics. Thus, the experimental results may differ from the models, also due to local peaks that distort performance, worsening the overall results.

Water in the cell undergoes several physical processes, the main ones of which have been described in the work of Anderson et al.: [55]

- Water condensation for decreasing temperature.
- Water condensation due to increasing pressure.
- Water condensation due to reached vapour pressure.
- Water transport from the anode to the cathode caused by electroosmotic drag.
- Water diffusion into the GDL due to an excessive production.
- Back diffusion from the cathode to the anode.

The first aspect I want to underline is the back diffusion process. It occurs when the produced water accumulates in correspondence of the cathode causing a concentration gradient. For this reason, the system tries to reach equilibrium through the water diffusion towards the anode. This process takes place in the opposite direction of electroosmotic drag. In order to better understand these processes, in figure 56 it is presented a schematization of the water management inside the cell.[56]

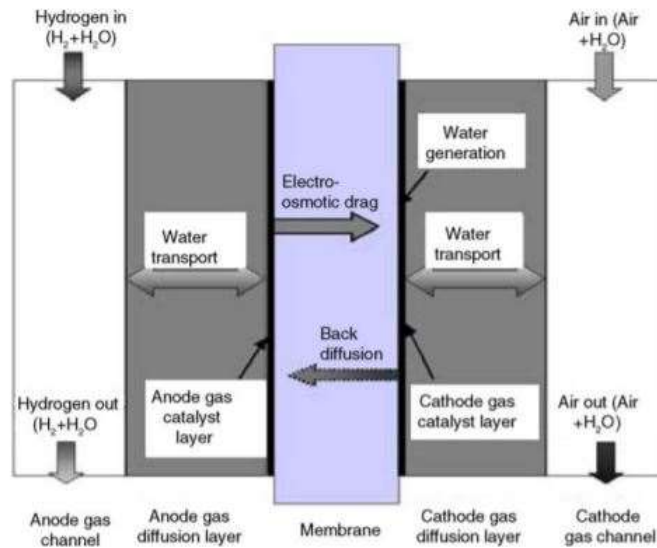


Figure 56 -Water transport [56]

The water flux two-phase management can modify pressure and it can create inhomogeneous water distribution altering PEMFC performances. In fact, the pressure drop is an indicator of the amount of liquid water present into the flow channel of PEMFCs. Indeed, as reported in the work of Anderson et al. [55], the increase of pressure is related to the increase of liquid water content that accumulates into the cell. In this way, pressure drop is a useful parameter to evaluate how the water transport inside the cell is acting and where any unwanted accumulation is concentrated.

Other important parameters related to the water transport phenomena are the inertial forces present into the system and the viscosity that can slow down the water transport. In relation to the last-mentioned properties, a pivotal role is assumed by the temperature which is able to decrease the viscous resistance of water. Also, the regulation of the temperature induces a regulation of the liquid water content.

The ideal goal would be to have the lowest possible level of liquid water in the cell, which should be slightly above the saturated vapor level, in order to ensure the perfect membrane humidification conditions.

As it has been demonstrated in this work through the simulations performed, a slightly increase in the temperature inside the cell improves cell's performances. One of the reasons for this improvement is due to the reduction in water content and it happens because when air heats up it is able to absorb a higher content of water vapor, storing it inside.

Anderson et al. argued the possibility to create a temperature gradient between anode and cathode sides to create a thermo-osmosis gradient able to regulate liquid water content. Another proposal is to create a pressure gradient that can control water migration.

Not only settings of physical parameters can adjust water content, but the geometrical aspect can also be used. For example, thin membranes encourage the back diffusion, but the right design of the membrane's thickness is a compromise with some other factors like the excessive quick drying and the mechanical strength.[55] Also the flow channel design can improve the water transport, as it has been demonstrated that serpentine flow fields create a correct pressure drop.

I would still like to discuss two elements related to cell construction that can improve water transport. The first of which is the construction of hydrophobic channels in the gas diffusion layer, which would make possible to increase the removal of water from the cell and consequently improve gas transport, as demonstrated in the previous work cited above. The second aspect relates to the cross-section of these channels: the size regulation of these channels allows the optimisation of pressure values useful for water removal.[55] Finally, another possibility for water regulation is the integration of electroosmotic pump to remove the excess of water more efficiently.

To understand how these theoretical aspects interact with each other in the reality of the cell, the model at our disposal allows us to evaluate water transport through different graphs.

As I previously did for current density distributions, I evaluated the comparison between the model output for Aquivion E87 and Nafion 211. The comparison is useful to highlight the various water flows behaviour for each membrane typology and the main differences related to flow development in the two membranes.[54]

All the figures reported below are referred to 353 K and 100% of relative humidity at current collectors. Figures 57 and 58 display the water gas flux trend into the gas diffusion layers and at the interfaces with catalyst layers. Comparing the graphs, you can clearly see for each of them that there is less oscillatory pattern into the gas diffusion layers and there is a kind of constant flow, except for the portions of the cell in contact with the catalyst layer.

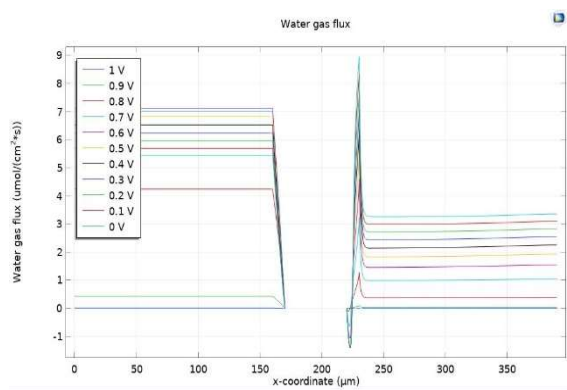


Figure 57 – Water gas flux, E-87

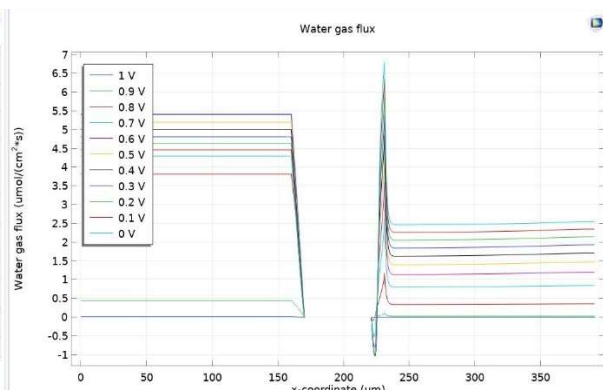


Figure 58 – Water gas flux, Nafion 211

The purpose of these graphs is to underline how the water content change at the interfaces with the active layers. In order to explain widely this aspect, figures below (figures 59-60) are useful to highlight how there is an increase in the production of water flow in the membrane layer. The cardinal factor that induces this process is the presence of the cathode catalyst layer that induces the closing of the cycle of cell reactions, having as final product the formation of water. Because of that, in figure 59 there is a huge peak in the middle of cathode catalyst layer (around 225 µm) and the same can be observed for figure 60. The centre of this layer represents the part where the catalyst reaches its highest concentration and purity and where it can most effectively activate the reactions.

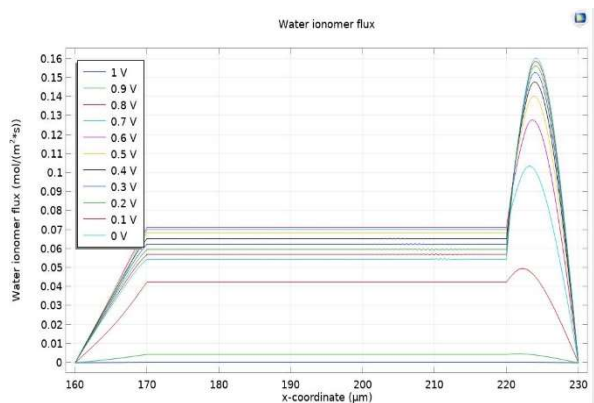


Figure 59 - Water ionomer flux related to catalytic and membrane layers E-87

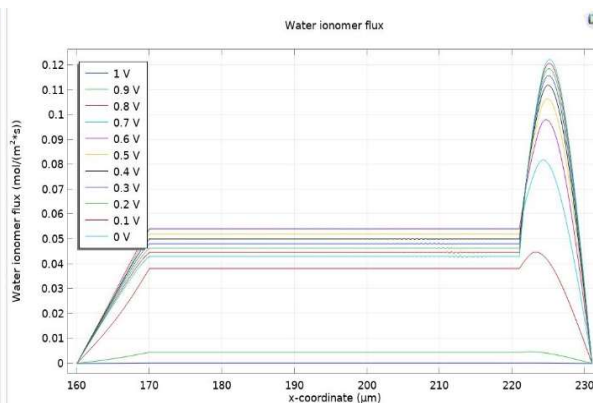


Figure 60 - Water ionomer flux related to catalytic and membrane layers, Nafion 211

Figures 61 – 62 show how liquid water flux has a different pattern into the cell. In these figures it is clear that there is no liquid water flux in the anode side. The only liquid water flux into the cell is on the cathode side and this flow increases in quantity in the cathode catalyst layer. This is perfectly in line with what will be discussed later: liquid water is expelled from the anode side of the cell by dedicated devices. Once past this layer, inside the membrane the water flow reaches an equilibrium situation and begins to be linear with no further fluctuations.

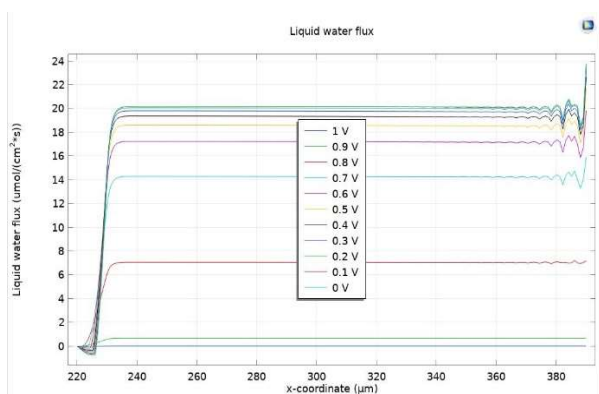


Figure 61 – Liquid water flux, E-87

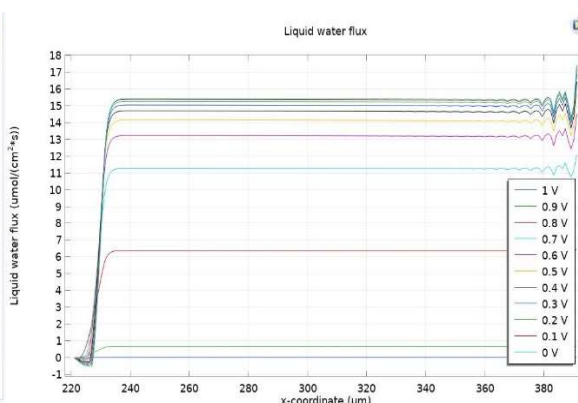


Figure 62 – Liquid water flux, Nafion 211

In figures above, liquid water transport comparison for Aquivion E-87 and Nafion 211 are displayed. The comparison of graphs demonstrate that trends are similar obviously with different values depending on the membrane's properties. This is valid for all the other comparison reported before. The only few variations are function of various membrane characteristics, which affect the efficiency of water transport.

As explained for oxygen transport, all these factors are linked together and the decrease of a fundamental parameter such as oxygen transport can only induce a parallel decrease in water formation. This, chemically speaking, is merely due to a stoichiometric ratio between reagents and products: as the transport of the reagent decreases, the formation of the product will necessarily decrease.

In figure 63, the water content of the ionomer for Aquivion E-87 is presented and the graph shows a lack of homogeneity in the thickness of the ionomer layer. Still looking at the same figure, different levels of voltage profile are plotted and they show a considerable variation in the water content within the ionomer. The water content is higher for low values of applied

voltage and high values of current density, whereas for high values of voltage the water content of the ionomer seems to reach an equilibrium.

To explain this behaviour, it is necessary to return to the analytical description of the water content of the ionomer, which was discussed in Chapter 2. The work of Yuan and Ou [54] defines the ionomer water content as: “the ratio of the number of water molecules to the number of charge (SO₃H⁺) sites” with the equation below:

$$\lambda = 0.043 + 17.81 * RH - 39.85 * RH^2 + 36.0 * RH^3$$

RH is determined by $\frac{x_{H_2O}}{x_{Sat}}$. When the relative humidity is saturated, the gas water becomes liquid water and liquid water will plug the pores, reducing reactions speed.[54]

Taking the curve with applied voltage of 0.6 V as example, there is a particular trend. In the anode catalyst layer the water content decreases until the membrane layer is reached: here the water content increases. The increase becomes bigger when the cathode catalyst layer is reached. This trend is due to the combination of different physical phenomena taking place in the cell. In fact, if it is true that there is a back diffusion phenomenon, there is also an electrochemical gradient pushing the water towards the cathode, increasing the water content. The reason why there is a reduction in water content on the anode side is explained in the work of Yuan et al. who state that at the anode of the cell the steam is in a saturated vapour condition so that water can be removed.[54]

Finally, I want to underline the increase in the presence of water inside the cathode catalyst layer due to the closing of the reaction cycle (at 220µm).

In figure 64, there are different ionomer water content behaviours studied by Ou and Yuan in the previous cited work for different values of voltage. I want to report this figure because it is worthwhile to show how water transport section in the model is validated into the literature. In fact, it displays the same curve trend of figure 63, with the reduction of water content into the anode catalyst layer (160/170 µm) and the increase of water content once this layer is overcome.

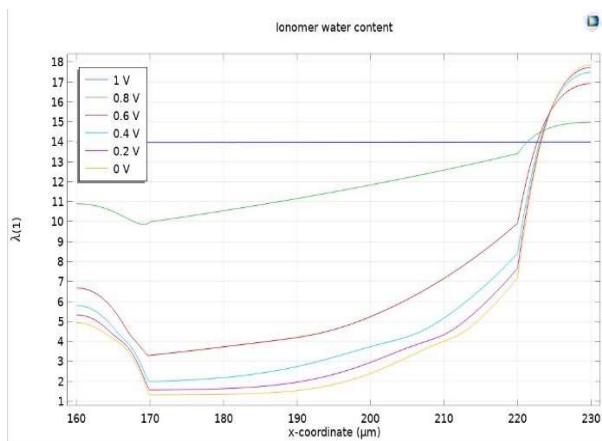


Figure 63 - Ionomer water content, E-87

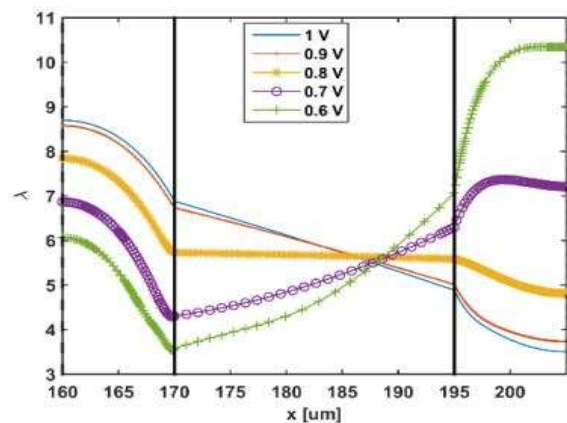


Figure 64 – Ionomer water transport validation [54]

A final mention must be made for the ion transport phenomena. To improve the transport of ions inside the cell, it is necessary to choose porous electrodes that allow the passage of ions by optimizing their transport through some sort of channels. The ions transport is related to the

other physical transport, so it is necessary to study how it is in relation with water transport. It should be emphasized that the mass transport of ions is a phenomenon that is widely discussed but that sees as a driving phenomenon the migration of the same caused by the potential applied on the cell.[57]

5.6. Proposals for enhancing cell parameters

In order to understand in which aspects are useful to invest considerable economic effort, research has to find out what the targets are. The main research goal is to achieve high current levels at high voltage levels, in order to maximize the power output.

Lots of papers describe in which areas it would be better to go deeper in the analysis, looking for possible future improvements and where it is most valuable to look for a better solution.

In this work, at page 16, it is available a first section of future development. It looks at the global cell output point of view while now I will analyse how to improve and which layers would be best to work to improve the performance of the membrane electrode assembly.

Starting from the thermal point of view, PEMFCs have high thermal efficiency, around 65%. This value and all those discussed before are referred to ideal conditions, but there are some degradation problems that must be taken into account and limited if we want to keep up target performances over the time. These degradations appear in different parts of the cell and to limit this aspect some strategy can be used:

- peak cathode potential reduction.
- high voltage. [47]

The first aspect is required to limit cathode catalyst degradation. The high voltage instead, it activates some consequences: at first high voltage induces high temperature conditions that prevents a longer life for electrode and membranes but high temperature induces different kinetics in the cell reactions and so different heat losses management is required.[47]

As mentioned, all the data analysed in this work are based on ideal conditions. But after several work cycles, the PEMFCs are inevitably subject to degradation, which could worsen the transport phenomena and therefore the performance.

During this work, different section for the catalyst ink deposition have been treated because the catalyst/membrane interface is a fundamental aspect to improve cell performances. In fact, if the catalytic state is able to activate oxidation and reduction reactions correctly, if it has been treated in such a way to increase the active surface area of the catalyst and if it is capable to encourage the passage of the various molecules, then the cell's performance will be improved. There are some issues if this does not occur, as it happens, for example, with the reduction of platinum that causes a reduction of voltage level preventing a proper oxygen transport.[48]

In other words, to improve cell parameters, great attention must be given to optimising of the system, especially of catalytic layer and its interface with the membrane. At first using the correct amount of platinum, which must be placed on the membrane to maximise the active surface area. Then by enhancing transport parameters, optimising the presence of liquid water: water content that if reduced does not allow correct wetting of the membrane with a consequent reduction in current transport, but in excess it occludes the pores and it does not allow correct

oxygen transport. Oxygen transport that is limited by the reduction of platinum, which it is necessary to keep costs down, avoiding massive exploitation of the substances.

As for the catalyst, great attention must be paid to optimising the membrane which, foremost, has to be able to improve the proton conductivity. In addition, my suggestions, from my limited experience, would be to evaluate these parameters not at 353 K, as it is done in the papers I have analysed and in the Solvay data sheets, but at 373 K, to start researching at higher temperatures in order to reduce degradation phenomena.

Improvements to the membrane also include the optimisation of transport phenomena: enhancement of water balance, improvement of back diffusion processes and oxygen transport. In addition, it is necessary to assess how interconnected these processes are and how they require an inclusive review of all aspects, through the use of models such as ours, which are capable of including all of them.

6. Conclusions

Proton exchange membrane fuel cells are not a recent technology anymore, yet they are still promising in terms of future development and commercialization.

Today, in the market a great number of different fuel cells are available, but the automotive market has already reached the convergence around PEMFCs for their low working temperature and for their fast start-up time, which is ideal for this kind of application.

There are already some automotive applications on our streets but the main issue to be overcome is a solid hydrogen distribution grid that can allow owners to refuel their car and to show the world that FC cars are not something related to the future but they can be a present solution.

In this work I explained some of the possible ink depositions, the importance of this passage to define the polarization curve and the consequence of this kind of graph to industrial development. After a brief passage in the Politecnico laboratory to see how the evaluation of parameters is performed, I used parameters evaluated from someone else to be more precise and to avoid excessive approximation.

In this work, I provide eight set of simulations changing for each set the temperature and moisture conditions. Every step of simulation was carried out for five different membranes available in the market. The main focus was related to produce a solid result through rigorous parameterisation of consolidated data from the literature.

Before performing the simulations, I had to understand how the model works and what kind of parameters have to be changed to perform a correct evaluation of the model. Among all the parameters, the most important one for the membrane layer is certainly the proton conductivity. A crucial passage before the simulation was the correct evaluation of this parameter with Arrhenius equation at reference temperature and moisture conditions.

At the end of preliminary passages, entering the correct values for each type of membrane, I was able to simulate the cell behaviour. The analysis of the results showed that the most performing membrane was the Aquivion E87. The first step after simulations was to validate simulations' results with the literature polarization and power curve. It was necessary to demonstrate the model's output results were of the same order of magnitude as those measured in the laboratory.

In the section of the discussion on simulation results the analysis of current distribution, oxygen and mass transport is inserted. These are some of the most important physical parameters to consider for a fuel cell. The way these phenomena interact with each other is the key to understand the internal cell dynamics and being able to work in the right direction to improve them. During this work, the comparison between Aquivion E-87 and Nafion 211 for current distribution, oxygen transport and water transport was carried out by looking at the graphs available in the model. In addition, curves available in the literature were also used for comparison in order to validate these parameters.

I would like to underline that all these simulations require solid experimental confirmation in the future with more precise evaluation of parameters. My work had the aim to highlight the existence of technologies that can compete or, as simulations have demonstrated, can be better

than Nafion. This is useful to demonstrate that the overwhelming monopoly of Nafion can be reduced thanks to new quality membranes that have recently been produced.

The competition in the market is fundamental because it stimulates, on the one hand, the research for performance and, on the other, a reduction in costs.

In the sector of fuel cells, the aspect of competition is not at all taken for granted as there are not many manufacturers. If one of these can produce the same component with higher performance, the market will surely converge in that direction, allowing the company to regulate prices independently; therefore, indirectly hindering the spread of the technology itself. Vice versa I believe that a healthy competition can push towards a common effort of each company to produce the best version of its product and thus the containment of rare metals use, the improvement of cell performances and the production costs optimization.

I strongly believe that the effort of research combined with the increasing necessity to accelerate the energy transition could give the final impulse to the creation of an alternative reality to the traditional motorization. A new technology that can be friendly with the planet we live on, without filling its atmosphere with pollutants and without triggering a new raid of rare minerals is possible and it is from today.

I started this course at Politecnico with the aim to be part of this change and I really hope that one day I will reread this work with the awareness of having been part of it in some way.

7. References

- [1] U.S. DEPARTMENT OF ENERGY: www.energy.gov/eere/fuelcells/types-fuel-cells.
- [2] “Electrochemical devices for energy: fuel cells and electrolytic cells”, M. Cassir, V. Lair; in Handbook of Membrane Reactors: Reactor Types and Industrial Applications, Science Direct; 2013.
- [3] “Using ultrasound to effectively homogenise catalyst inks – Is this approach still acceptable?”; B. G. Polleta and S. S. Kocha; 2021.
- [4] “Multi-year Research, Development and Demonstration Plan (Fuel Cells Section) - Fuel cell technologies office”; DOE USA; 2016.
- [5] UNFCCC, United Nations Framework Convention on Climate Change: <https://unfccc.int/process/bodies/supreme-bodies/conference-of-the-parties-cop>.
- [6] EUROPEAN COMMISSION: https://ec.europa.eu/clima/policies/international/negotiations/paris_it.
- [7] “How our daily travel harms the planet”; Jocelyn Timperley; BBC; 2020.
- [8] Center for climate and energy solutions, <https://www.c2es.org/content/international-emissions>.
- [9] International Energy Agency IEA, www.iea.org/data-and-statistics/charts/global-energy-related-co2-emissions-1990-2021.
- [10] “A review on the key issues of the lithium-ion battery degradation among the whole life cycle”; X. Han, L. Lu; Science Direct; Volume 1; 2019.
- [11] CNBC, <https://www.cnbc.com/2021/06/17/bmw-starts-european-road-tests-of-hydrogen-fuel-cell-cars.html>.
- [12] The Fuel Cell Industry “Review 2020”, E4tech.
- [13] TOYOTA, <https://www.toyota.it/gamma/mirai/nuova-mirai>.
- [14] “Designing the next generation of proton-exchange membrane fuel cells”; K. Jiao, J. Xuan, Q. Du1, Z. Biao, B. Wang et al.; Perspective; 2021.
- [15] TOYOTA, <https://global.toyota/en/detail/300475>.
- [16] “A practical Equivalent Electrical Circuit model for Proton Exchange Membrane Fuel Cell (PEMFC) systems”; O. Atlam, G. Dundar; ScienceDirect; 2021.

- [17] “Thermodynamic and economic study of PEMFC stack considering degradation characteristic”; X. Chen, J. Xu; Elsevier; 2021.
- [18] “Catalyst Slurry Preparation Using a Hydrodynamic Cavitation Dispersion Method for Polymer Electrolyte Fuel Cells”; H. Kuroki, K. Onishi; Ind. Eng. Chem. Res. 2019.
- [19] “Free open reference implementation of a two-phase PEM fuel cell mode”; R. Vetter, J. O. Schumacher; Elsevier; 2018.
- [20] “Modelling the Proton-Conductive Membrane in Practical Polymer Electrolyte Membrane Fuel Cell (PEMFC) Simulation: A Review”; E.J. F. Dickinson, G. Smith, Membrane; 2020.
- [21] “Data classification with the Vogel – Fulcher – Tammann – Hesse viscosity equation using correspondence analysis”; M. L. F. Nascimento, C. Aparicio; ScienceDirect; 2007.
- [22] “Absorption, Desorption, and Transport of Water in Polymer Electrolyte Membranes for Fuel Cells”; Shanhai Ge et al; J. Electrochemical. Society; 2005.
- [23] Proportions described by the analyses conducted by Professor Monteverde.
- [24] “Performance Comparison of Proton Exchange Membrane Fuel Cells with Nafion and Aquivion Perfluorosulfonic Acids with Different Equivalent Weights as the Electrode Binders”; T. Li, J. Shen, G. Chen, S. Guo; ACS OMEGA; 2020.
- [25] “Enhanced Proton Conductivity of a Zn (II) -Based MOF/Aquivion Composite Membrane for PEMFC Applications”; S. Paul, S. J. Choi; Energy&Fuel; 2020.
- [26] “How the Morphology of Nafion-Based Membranes Affects Proton Transport”; Lufrano, Simari, Di Vona; Polymers; 2021.
- [27] “On the evolution of proton conductivity of Aquivion membranes loaded with CeO₂ based nanofillers: Effect of temperature and relative humidity”; A. Donnadio, R. D’Amato; Journal of power sources; 2018.
- [28] “Electro-osmotic drag coefficient and proton conductivity in Nafion membrane for PEMFC”; Z. Luo a, Z. Chang; Science Direct,2009.
- [29] “Depression of proton conductivity in recast Nafion® film measured on flat substrate”, Z. Siroma, R. Kakitsubo; Journal of power Sources; 2009.
- [30] “Properties of Nafion NR-211 membranes for PEMFCs”; J. Peron, A. Mani; Journal of power Sources; 2010.
- [31] “New modified Nafion-bisphosphonic acid composite membranes for enhanced proton conductivity and PEMFC performance”; F. Texeira, A. de Sa; Science Direct; 2020.

- [32] “Cerium Stabilized by Titanium Carbide as a Sustainable Filler in the Nafion Matrix Improves the Mechanical Integrity, Electrochemical Durability, and Hydrogen impermeability of Proton-Exchange Membrane Fuel Cells: Effects of the Filler Content”; M. Vinothkannan, S. Ramakrishnan; Applied material and interfaces; 2020.
- [33] “Facilitating Proton Transport in Nafion-Based Membranes at Low Humidity by Incorporating Multifunctional Graphene Oxide Nanosheets”; X. He, G.Zhao; Applied material and interfaces; 2017.
- [34] “Performance improvement of self-humidifying PEM fuel cells using water injection at various start-up conditions”; D. Cha, W. Yang, Y. Kim; Energy; 2019.
- [35] “Comparative Experimental Study on Ionic Polymer Membrane Composite based on Nafion and Aquion Membrane as Actuators”; B. Luo, Z. Chen; IOP Conference Series: Materials Science and Engineering; 2017.
- [36] “Aquion Ionomer in Mixed Alcohol–Water Solution: Insights from Multiscale Molecular Modeling”; A. Malek, E. Sadeghi; J. Jankovic; The Journal of physical chemistry; 2020.
- [37] “A Comparative Study of Water Uptake by and Transport Through Ionomeric Fuel Cell Membranes”; T. Zawodzinski, Jr. Springer; Journal of electrochemical Society; 1993.
- [38] “Polymer electrolyte fuel cell model”; T. Springer, T. Zawodzinski; Journal of electrochemical Society; 1991.
- [39] “Aquion – Poly (N-vinylcarbazole) Holistic Flory –Huggins Photonic Vapor Sensors”; H. Megahd, C. Oldani; Advance Optical Materials; 2021.
- [40] “Molecular dynamics simulation study on the effect of perfluorosulfonic acid side chains on oxygen permeation in hydrated ionomers of PEMFCs”; S. H. Kwon, H. Kang; Scientific Report; 2021.
- [41] “Synthesis and performance of solid proton conductor molybdovanadosilicic acid”; Z. Xie, H. Wu; RSC advances; 2018.
- [42] “Comparative study of sulfonated branched and linear poly(phenylene)s polymer electrolyte membranes for fuel cells”, F. Ahmed, S. Chadra; Science Direct; 2017.
- [43] AQUIVION E87 technical data sheet, www.solvay.com.
- [44] AQUIVION E98-05 technical data sheet, www.solvay.com.
- [45] AQUIVION E98-09S technical data sheet, www.solvay.com.
- [46] M. Santarelli, 28-10-2020 lesson.

- [47] “New roads and challenges for fuel cells in heavy-duty transportation”; D. A. Cullen, K. C. Neyerlin, R. K. Ahluwalia, R. Mukundan, K. L. More, R. L. Borup, A. Z. Weber, D. J. Myers, A. Kusoglu; Nature energy; 2021.
- [48] “The role of oxygen-permeable ionomer for polymer electrolyte fuel cells”; R. Jinnouchi and K. Kudo, K. Kodama, N. Kitano, T. Suzuki, S. Minami, K. Shinozaki, N. Hasegawa, A. Shinohara; Nature communication; 2021.
- [49] “Analysis of the cathode side of a PEMFC varying design parameters to optimize current distribution and power density”; T. Falagüerra, P. Muñoz, G. Correa; ELSEVIER; 2020.
- [50] “Current Distribution Mapping for PEMFCs”; V. Lilavivata, S. Shimpaleea; Elsevier; 2015.
- [51] “Influence of platinum dispersity on oxygen transport resistance and performance in PEMFC”; X. Sun, H. Yu; ELSEVIER; 2019.
- [52] “Cross-dimensional model of the oxygen transport behavior in low-Pt proton exchange membrane fuel cells”; J. Liang, Y. Li; Chemical Engineering Journal; 2020
- [53] Fuel cell photo taken by www.genitronsviluppo.com.
- [54] “Analyzing and Modeling of Water Transport Phenomena in Open-Cathode Polymer Electrolyte Membrane Fuel Cell”; W.W. Yuan, K. Ou; Applied Sciences; 2021.
- [55] “A critical review of two-phase flow in gas flow channels of proton exchange membrane fuel cells”; R. Anderson, L. Zhang; Journal of Power Sources;2010;
- [56] “Investigation of water transport through membrane in a PEM fuel cell by water balance experiments”; Q. Yan, H. Toghiani; Science Direct; 2005.
- [57] “Mass Transport in Gas-Diffusion Electrodes: A Diagnostic Tool for Fuel- Cell Cathodes”; M. L. Perry, J. Newman; Electrochemical Society;1998.